# Surface Chemistry of Transition Metal Carbides

Henry H. Hwu[†] and Jingguang G. Chen*[,‡]

*Department of Materials Science and Engineering, Department of Chemical Engineering, Center for Catalytic Science and Technology (CCST), University of Delaware, Newark, Delaware 19716*

*Received March 17, 2004*

## Contents



Henry H. Hwu received his B.S. degree in chemical engineering from MIT in 1998. He received his Ph.D. degree in materials science and engineering from the University of Delaware in 2003, focusing on the surface chemistry of transition metal carbides. He then spent one year in Singapore's Institute of Bioengineering and Nanotechnology as a research scientist, working on silica–apatite composites for load-bearing orthopedic implants. He is now back at the University of Delaware as a postdoctoral fellow, examining bimetallic systems for potential use as a fuel cell cathode. His research interests include catalytic combustion, surface chemistry, and artificial bone implants.

Jingguang G. Chen received his B.S. degree in chemistry from Nanjing University, China, in 1982. He received his Ph.D. degree in chemistry from the University of Pittsburgh in 1988. He then spent one year as a postdoctoral fellow in KFA-Julich, Germany. He joined the Exxon Corporate Research Laboratory in 1989. In 1998 he acepted a faculty position at the University of Delaware. Currently, he holds the positions of Professor of Chemical Engineering and Director of the Center for Catalytic Science and Technology (CCST). His primary research interest is the understanding and discovery of novel catalytic materials using a combination of surface science, theoretical modeling, and reactor studies.

## 1. Introduction

Transition metal carbides (TMCs) are produced by incorporating carbon atoms into the interstitial sites of their parent metals, which typically include all 3d elements and 4d/5d elements of groups 3−6 early transition metals. In general, TMCs of early transition metals possess unique physical and chemical

* Corresponding author. E-mail: jgchen@udel.edu.
[†] Department of Materials Science and Engineering.
[‡] Department of Chemical Engineering.

10.1021/cr0204606 CCC: $53.50 
Published on Web 12/21/2004

properties.[1−6] For example, TMC compounds combine the physical properties of three different classes of materials: covalent solids, ionic crystals, and transition metals. As a result, TMC compounds often demonstrate the extreme hardness of covalent solids, the high melting temperature of ionic crystals, and the excellent electric and thermal conductivity of transition metals. The unique combination of these desirable physical properties has led to the commercial applications of TMCs as cutting tools[1] and hard-coating materials.[3]

In addition, TMCs of groups 4−6 early transition metals are characterized by many unique and intriguing catalytic properties. Ever since the landmark paper by Levy and Boudart regarding the Pt-like properties of tungsten carbides,[7] the catalytic properties of TMCs have been the subject of many investigations in the fields of catalysis and surface science. From the catalysis literature it is now well established that the catalytic properties of TMCs often show strong similarity to those of the more expensive Pt-group metals (Ru, Rh, Pd, Os, Ir, and Pt).[6] In particular, in reactions involving the transformation of C−H bonds of hydrocarbons, such as dehydrogenation, hydrogenation, and hydrogenolysis, the catalytic performances of TMCs are approaching or surpassing those of Pt-group metals.[2,5,6] The catalytic and electrocatalytic properties of group 6 carbides have also been the subject of many investigations because of their potential application as alternative electrocatalysts in hydrogen and methanol fuel cells.[8−11]

Experimental and theoretical surface science studies have played an important role in confirming and understanding the similar surface properties of TMCs to those of Pt-group metals. In particular, TMC surfaces offer excellent model systems to determine how the electronic properties of metal surfaces are modified by the incorporation of carbon and how the electronic modifications in turn alter the surface chemical properties. The objectives of the current review are primarily twofold: (1) to demonstrate the general similarities and differences in the surface chemistry of TMC surfaces and (2) to correlate the chemical properties with the underlying electronic properties of TMC surfaces.

There were several comprehensive reviews on the various properties of TMCs. Johansson reviewed the electronic properties of bulk single-crystal TMCs in 1995.[12] The chemical and catalytic properties of powder and supported TMC catalysts were reviewed by Oyama in 1996.[5] The preparation, characterization, and reactivities of TMC surfaces were reviewed by Chen in 1996.[6] The characterization of the local structural and electronic properties of single-crystal and polycrystalline TMCs was reviewed by Chen in 1997.[13]

The scope of the current review will focus on the electronic and chemical properties of well-characterized TMC surfaces. After briefly describing the preparation and characterization of TMC surfaces in section 2, we will systematically review the chemical properties of TMC surfaces in sections 3−7. The review will be concluded by discussion of correlating electronic properties with chemical activities in section 8 and future research directions in section 9. The results to be discussed in the current review include those published after 1996, as well as selected earlier publications related to the topics of this review. The readers should find more systematic and comprehensive discussions of results published before 1996 in earlier reviews.[5,6,12,13]

## 2. Characterization of Carbide Surfaces

### 2.1. Common Carbide Surface Structures

The groups 4 and 5 TMCs all form monocarbides (TiC, ZrC, HfC, VC, NbC, and TaC) with a face-centered-cubic (fcc) B1 crystal structure.[14] Similar to the NaCl structure, these carbides are characterized by two interpenetrating metal and carbon fcc lattices. The most commonly studied crystalline planes are the (100) and (111) surfaces. The (100) surface is characterized by the coexistence of the metal and carbon atoms. The (111) orientation has alternating layers of metal and carbon atoms, and the (111) surface can be terminated either by metal or by carbon. The structures of the metal- and carbon-terminated fcc(111) surfaces are illustrated in Figure 1a and b, respectively.

In comparison, group 6 metals (Cr, Mo, W) do not always produce stable monocarbides. The most commonly studied group 6 TMCs include $Mo_2C$, $W_2C$, and WC. In general, the structures of group 6 TMCs are much more complex than their groups 4 and 5 counterparts. For example, the $\beta$-$Mo_2C$ phase has an orthorhombic crystal structure,[15] with the (100) surface corresponding to the closest-packed surface that can be terminated by either Mo or C atoms. Because the arrangement of Mo is only slightly distorted from a hexagonal-closed packed (hcp) arrangement, the crystal structure of $\beta$-$Mo_2C$ can often be loosely described as an hcp structure with carbon atoms occupying the octahedral interstitial sites. Correspondingly, the closest-packed surface of $\beta$-$Mo_2C$ is often reported in the literature as the hcp(0001) surface. The structures of the Mo- and C-terminated $\beta$-$Mo_2C$(0001) surfaces are illustrated in Figure 1c and d, respectively.

### 2.2. Preparation of Carbide Surfaces

Surface science studies have been primarily focused on three types of materials: bulk single crystal carbides, carbide-modified single crystal metal surfaces, and polycrystalline carbide thin films. There are advantages and disadvantages for using each type of materials. The main advantage for using bulk crystals is their well-ordered stoichiometric surfaces; the disadvantage is the scarcity of the crystal materials, especially for group 6 TMCs. The advantage for carbide-modified metal surfaces is the ability to control the carbon/metal stoichiometry and to directly compare with the parent metal surfaces; the disadvantage is the imperfect termination and defects. The advantage of studying thin films is the op-

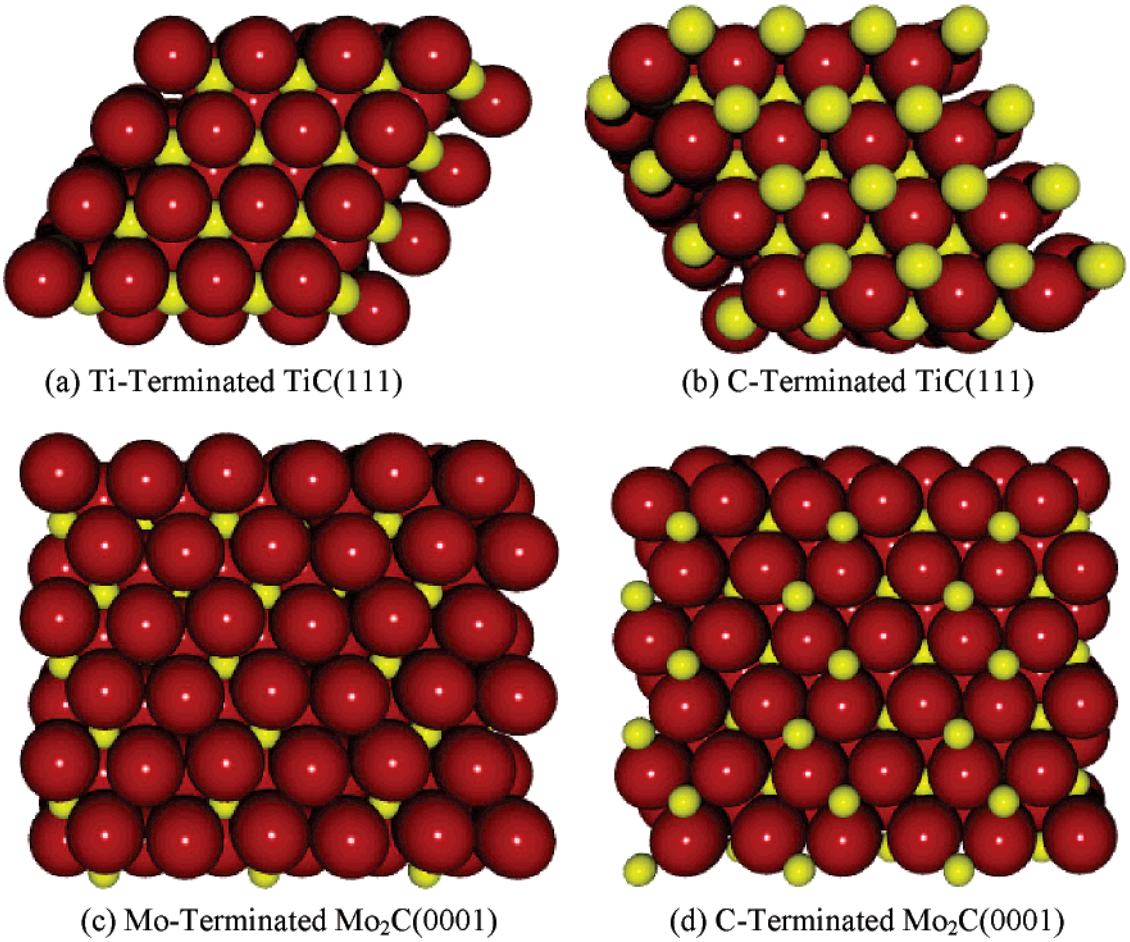


**Figure 1.** Surface structures of carbon- and metal-terminated TiC(111) and $Mo_2C$(0001), which represent the most close-packed surfaces of TiC (fcc structure) and $Mo_2C$ (hcp structure), respectively. The smaller spheres represent carbon atoms, which reside either below (in parts a and c) or above (in parts b and d) the metal surfaces.

portunity to address the so-called "materials gap" to correlate single crystals with more realistic polycrystalline materials; the disadvantage is the lack of general understanding of the surface properties.

The preparation of clean surfaces of bulk carbides typically involves the sputtering and annealing cycles that are commonly used for metal surfaces.[12] It is important to point out that the surface structures of TMCs are often different from those of the bulk materials. For example, the contraction and relaxation in the first interlayer spacing often occur for the fcc(111) and fcc(100) carbide surfaces. In addition, the surface carbon/metal stoichiometries also depend on the annealing temperature. More detailed discussion about the preparation and characterization of bulk single-crystal TMCs can be found in a previous review.[12]

The preparation of carbide-modified surfaces is generally achieved by exposing the clean metal surfaces to unsaturated hydrocarbons, followed by annealing to temperatures higher than 1000 K.[6] The annealing procedure is often required to drive the excess surface carbon into the interstitial sites. In most cases, well-ordered surface structures, as determined using low-energy electron diffraction (LEED), can only be obtained after annealing. The exposing−annealing cycles are typically repeated several times to obtain the desirable carbon/metal stoichiometries and/or surface structures. The specific procedures for preparing carbide-modified surfaces, as well as the corresponding LEED patterns, have been described in detail in an earlier review[6] and will not be discussed in the current review.

The preparation of polycrystalline thin films has been achieved in two ways: carburization of metal films with hydrocarbons[16] or physical vapor deposition (PVD) from a bulk carbide target.[17] For example, a $\beta$-$Mo_2C$ thin film was prepared by carburizing a Mo foil at high temperatures with a mixture of methane and hydrogen, followed by room-temperature passivation in a flow of 0.5% $O_2$/He.[16] X-ray diffraction (XRD) measurements indicated that the foil was essentially pure $\beta$-$Mo_2C$. In the PVD method, thin films of carbides were prepared by magnetron sputtering from carbide targets onto a flat substrate, such as glassy carbon or single-crystal sapphire. Thin films of $W_2C$ and WC were recently prepared by sputtering from a bulk WC target, and the desirable carbide phases were obtained by controlling the deposition temperature and postannealing conditions.[17] XRD measurements confirmed the phase purity of $W_2C$ and WC films. Similar to the case of bulk carbide single crystals, the surfaces of the carbide films can be cleaned by repeating cycles of sputtering and annealing.

**Table 1. Characterization of TMC Surfaces**

| | techniques |
|---|---|
| bulk carbides | |
| HfC(111) | ARPES,[24] ICISS[76] |
| α-$Mo_2C$(0001) | ARPES,[48] LEED,[45,48] STM,[45,47] XPS[45,48] |
| MoC(001) | DFT[238] |
| NbC(111) | AES,[33] ARPES,[28,29,77] CLPES,[29,33] ICISS,[75] STM,[66] UPS[188] |
| NbC(100) | CLPES,[30] LEED,[18] STM,[18,66] UPS[188] |
| TaC(111) | ARPES[77] |
| TiC(100) | AFM,[35] DFT,[20,34] HREELS,[85,193] LEED,[18,19] XPS[35] |
| TiC(111) | ARPES,[21,79] ARUPS,[74,97] ARXPS,[97] DFT,[20,22,31,34,73] ISS,[97,98] STM[73,88] |
| TiC(001) | ARXPS,[96] DFT,[39,42,62] ISS,[96] LEED,[96] UPS[96] |
| VC(100) | AFM,[35,86,181] DFT,[34,64] HREELS,[85,193] LEED,[86] STM,[86,181] XPS[35] |
| VC(110) | LEED,[65] STM[65] |
| WC(0001) | AES,[46,89] ARUPS,[89] CLPES,[90] DFT,[31,49] LEED,[46,174] STM[46] |
| ZrC(100) | ARPES,[27] LEED,[18] UPS,[82,104] XPS[82] |
| ZrC(111) | ARPES,[23,25,26,78] DFT,[63] SXPS,[83] UPS,[83,104] XAS,[32] |
| carbide-modifed surfaces | |
| C/Ti(0001) | AES[94] |
| C/Mo(100) | AES,[50,67,117] LEED,[117] microcalorimetry[50] |
| C/Mo(110) | AES,[51,53,54,58] DFT,[61] HREELS,[55] NEXAFS,[53,55,58,60] IRAS,[52] LEED,[51,216] SXPS,[55] XPS[53,58] |
| C/Ni/Pt(111) | AES,[153] NEXAFS,[153] XPS[58] |
| C/Ni(111) | LEED,[164] STM[164,165] |
| C/Ta(100) | AES[68] |
| C/V(110) | AES,[57,100] HREELS,[100] NEXAFS,[56,58,100,130] XPS[58] |
| C/W(111) | AES,[155] HREELS,[95,155,156] LEED[155] |
| C/W(100) | AES[69] |
| C/W(110) | AES,[156,157] HREELS[156] |
| C/W(211) | AES,[130] HREELS[130] |
| carbide thin films | |
| $Cr_xC_y$ | AES,[70] RHEED,[70] THEED[70] |
| $Mo_2C$ | UPS,[43] XPS[43] |
| β-$Mo_2C$ | XRD[16] |
| WC/$W_2C$ | XPS,[17,44] XRD[17] |
| carbide clusters | |
| $Co_2C_n^-$ | DFT,[71] PES[71] |
| $Mo_8C_{12}$ | DFT,[40,237] |
| $Mo_mC_n$ | TOF-MS[235] |
| $Ti_8C_{12}$ | DFT,[39,40,237] IR−REMPD,[38] IR−REMPI,[36] MS[36,38] |
| $Ti_{14}C_{13}$ | DFT,[39] IR−REMPI,[36] MS[36] |
| $Ti_mC_n$ | DFT[41] |
| $V_2C_n^-$ | DFT,[71,72] PES[71] |
| $V_nC_n$ | IR−REMPI,[37] MS[37] |

## 2.3. Common Characterization Techniques for Carbide Surfaces

The structural and electronic properties of carbide surfaces have been studied using a variety of experimental techniques and theoretical modeling. Table 1 summarizes the carbide surfaces that will be discussed in the current review. Table 1 also summarizes the experimental and theoretical techniques that have been utilized to characterize the electronic and structural properties of the corresponding surfaces. Discussion about the characterization of many other carbide surfaces, published before 1996, can be found in previous reviews.[6,12] In this section we will use the characterization of several carbide surfaces as examples to describe some of the most commonly utilized surface techniques. We will focus primarily on the characterization of the structural and electronic properties, which will be frequently referred to in later sections in the discussion of chemical activities of the corresponding carbide surfaces.

### *2.3.1. Groups 4 and 5 Carbides*

The TiC(100) surface has been examined using LEED[18,19] and theoretical calculations.[20] Tagawa and co-workers determined that the surface atomic structure of TiC(100) was relaxed, with the topmost C atoms displaced outward and the Ti atoms inward.[18,19] Jansen and Hoffmann conducted a comprehensive study of the TiC(100) and (111) surfaces by using extended Hückel tight binding calculations.[20] The TiC(111) surface has been studied with synchrotron-based, angle-resolved photoemission spectroscopy (ARPES), where the results showed the surface to be polar with the Ti layer on top.[21] Through local density of states (LDOS) calculations, Tan et al. showed that, at elevated temperatures (∼1900 K), the TiC(111) surface should always be Ti-terminated as a direct consequence of the different evaporation rates between C and Ti atoms.[22]

As summarized by Johansson,[12] photoemission spectroscopy (PES) measurements have revealed that the electronic structures of many fcc(111) surfaces were characterized by the existence of surface states near the Fermi level ($E_F$). In contrast, the density of states around the $E_F$ was relatively small on the fcc(100) carbide surfaces.[12] Such a difference in the surface states has been cited as the reason for the observations that the fcc(111) surface is generally more active than the fcc(100) of the same carbide.[23]

Edamoto and co-workers have utilized angle-resolved and core-level photoemission spectroscopy

(CLPES) to compare the surface electronic structures of the (111) surfaces of several groups 4 and 5 carbides, HfC(111),[24] ZrC(111),[23,25,26] ZrC(100),[27] NbC(111),[28,29] and NbC(100).[30] For example, ARPES data revealed the presence of a surface state near the Fermi level on HfC(111). On the basis of the resonance photoemission measurements as well as additional polarization-dependent studies, the surface state was attributed to the 5d orbitals of the surface Hf atoms.[24] These results agreed well with a previous investigation of the presence of the 3d states on TiC(111).[31] Additional measurements monitoring the effect of potassium[25] and cesium[32] adsorption on ZrC(111), and sodium,[29] potassium,[28] and cesium[33] adsorption on NbC(111) also revealed the intrinsic differences between the electronic structures of the groups 4 and 5 TMC surfaces.

Perry and co-workers have performed density functional theory (DFT) calculations on stoichiometric clusters to compare the electronic properties of TiC(100) and VC(100).[34] Clusters modeling the TiC(100) surface did not show the presence of occupied molecular orbitals with clear predominance of 3d character. Furthermore, the strong covalency between the C 2p and Ti 3d states could also limit the availability of these electrons for surface reactions. In contrast, using $V_9C_9$ clusters to model the VC(100) surface, these authors identified the occupation of predominantly metal 3d levels, leading to the equivalent of a $d^1$ electron configuration.[34] The frictional properties of TiC(100) and VC(100) were also compared with atomic force microscopy (AFM) measurements.[35] Perry et al. showed that the TiC(100) surface exhibited inherently lower friction than VC(100) by conducting measurements at various degrees of oxidation and humidity, as well as with several probe tips.[35] These results again pointed out differences in the electronic properties between groups 4 and 5 TMC surfaces.

Several recent theoretical and experimental studies have compared the low-index carbide single crystals with nanocrystals and "metcar" structures.[36−41] First principles calculations on TiC(001) showed that the surface C atoms moved slightly outward and Ti atoms inward,[39,42] consistent with experimental observation for the TiC(100) surface.[18,19] Rodriguez and co-workers recently determined that the structure of the $T_8C_{12}$ "metcar" consisted of metal atoms occupying the low-coordination inner positions and high-coordination outer positions, as well as the presence of six pairs of short C−C bonds. The presence of the $C_2$ groups increased the stability of the "metcar" $T_8C_{12}$ structure. In addition, the presence of these $C_2$ groups also enhanced the chemical reactivity of the Ti atoms by weakening the Ti−C bonds.[39]

### 2.3.2. Group 6 Carbides

The Mo and W carbide surfaces have been studied using ultraviolet photoelectron spectroscopy (UPS),[43] X-ray photoelectron spectroscopy (XPS),[43−45] scanning tunneling microscopy (STM),[46,47] LEED,[45,46] and Auger electron spectroscopy (AES).[46] For example, studies of α-$Mo_2C$(0001) revealed that the surface could be altered between Mo- and C-terminated simply by changing the annealing temperature.[45] Otani and co-workers used ARPES to show that the valence band region of a C-terminated α-$Mo_2C$(0001) surface consisted of Mo 4d, C 2s, and Mo 4d−C 2p hybrid bands.[48] Göthelid and Janin combined the STM, AES, and LEED techniques to study the structure of WC(0001) as a function of surface composition.[46] These authors reported a variety of LEED patterns, all of which were strongly dependent on the atomic C/W ratio at the surface.[46]

The interaction of Mo or W carbides with another metal has also been investigated to determine the underlying structural and electronic properties of the carbide surfaces. For example, an ab initio study involving the interface of Al(111) and WC(0001) has been reported by Siegel and co-workers.[49] It was determined that the ideal work of adhesion on the C-terminated WC(0001) surface was ~2 J/m$^2$ stronger than that on the W-terminated surface, confirming the effect of termination on the properties of the carbide surfaces. In another example, Campbell and co-workers have examined the adsorption energy of Pb on an ordered (1 × 1) $Mo_2C$ film on Mo(100).[50] AES and LEED studies confirmed that the carbide film contained one carbon per surface Mo(100) atom sitting in or near the fourfold hollow sites. The microcalorimetry measurements showed a large initial heat of Pb adsorption, which was consistent with $Mo_2C$ resembling a late transition metal chemically and/or electronically.[50]

Among the carbide-modified surfaces, the C/Mo(110) surface is one of the most thoroughly characterized.[13,51−55] LEED studies have revealed a p(4 × 4) pattern after the C/Mo(110) surface was annealed to 1000 K or higher.[51,54] AES measurements showed the C/Mo atomic ratio approaching 0.5, indicating a $Mo_2C$ stoichiometry for the surface carbide layer.[51,53,54] The electronic properties of the C/Mo(110) surface have been characterized using two synchrotron-based spectroscopies, soft X-ray photoelectron spectroscopy (SXPS)[55] and near-edge X-ray absorption fine structure (NEXAFS).[13,53,55] The SXPS results revealed that the density of states below the $E_F$ level was significantly different between C/Mo(110) and clean Mo(110), indicating an electronic modification upon the formation of carbides. NEXAFS has been utilized to determine the local bonding environment of carbon atoms, as well as the density of states above the $E_F$ level, of many groups 4−6 TMCs,[13,56−60] including the C/Mo(110) surface. For example, on the basis of the polarization dependence of C K-edge features,[55] NEXAFS results suggested that the C/Mo(110) surface was terminated by C atoms in a similar way as the C-terminated $Mo_2C$ surface shown earlier in Figure 1d. Results from recent DFT modeling were also consistent with the structural model of describing the C/Mo(110) surface as C-terminated $Mo_2C$/Mo(110).[61]

In the next five sections, we will systematically review the chemical activities of TMC surfaces toward different classes of inorganic and organic molecules. Table 2 provides of a summary of the reactions of molecules on different TMC surfaces, as well as the experimental and theoretical techniques that

**Table 2. Summary of Surface Chemistry on TMC Surfaces**

| surface | molecule(s) | technique |
|---|---|---|
| HfC(111) | $H_2/D_2$ | HREELS,[80] ICISS[76] |
| | $O_2$ | ARPES,[24] ICISS[76] |
| α-$Mo_2C$(0001) | $O_2$ | AES,[92] ARPES,[48] LEED,[92] TPD[92] |
| | CO | AES,[92] LEED,[92] TPD,[92] UPS[92] |
| | $C_4H_4S$ | DFT,[232] TPD,[210] UPS,[210] XPS[210] |
| C/Mo(111) | $CH_2I_2$ | HREELS,[137] TPD,[137] XPS[137] |
| | $CH_3I$ | HREELS,[136] TPD,[136] XPS[136] |
| | $C_2H_5I$ | HREELS,[137] TPD,[137] XPS[137] |
| C/Mo(110) | $H_2$ | TPD[61] |
| | $O_2$ | HREELS,[55] NEXAFS,[55] SXPS,[55] TPD[55] |
| | $H_2O$ | HR TPD,[182] EELS[182] |
| | $H_2S$ | SXPS,[212] NEXAFS[212] |
| | $SO_2$ | SXPS,[212] NEXAFS[212] |
| | CO | HREELS,[54] IRAS,[52] TPD[54] |
| | $CH_3OH$ | HREELS,[55,182] TPD[55,182] |
| | $CH_3SH$ | SXPS,[212] NEXAFS[212] |
| | $C_2H_4$ | AES,[126] HREELS,[55,58,126] TPD[55,58,126] |
| | $C_2H_6S$ | AES,[216] TPD[216] |
| | $C_2H_6S_2$ | AES,[217,218] TPD[217,218] |
| | $C_4H_4S$ | SXPS[211] |
| | $C_4H_8$[a] | HREELS[142] |
| | $C_4H_8$[b] | HREELS[142] |
| | $C_4H_8$[c] | HREELS,[58,145] TPD[145] |
| | $c$-$C_5H_8$ | HREELS,[53] TPD[53] |
| | $C_6H_6$ | HREELS,[172] TPD[172] |
| | $c$-$C_6H_8$ | HREELS,[153] TPD[153] |
| | $c$-$C_6H_{10}$ | HREELS,[55,152,153] TPD[55,58,152,153] |
| | $c$-$C_6H_{12}$ | HREELS,[167] TPD[167] |
| C/Mo(100) | $H_2$ | TPD[117] |
| | CO | TPD[117] |
| | $CO_2$ | HREELS,[197] TPD,[197] XPS[197] |
| | $C_2H_4$ | AES[125] |
| | $C_3H_5I$ | HREELS,[147] TPD,[147] XPS[147] |
| | $c$-$C_3H_6$ | TPD[166] |
| | $C_3H_7I$ | HREELS,[146] TPD,[146] XPS[146] |
| | $C_4H_4S$ | AES,[209] TPD[209] |
| | $C_4H_6$ | TPD[209] |
| | $C_4H_{10}$ | TPD[209] |
| | $C_6H_5I$ | HREELS,[175] TPD,[175] XPS[175] |
| C/Mo/W(111) | NO | TPD[120] |
| β-$Mo_2C$ foil | $O_2$ | XPS[16] |
| | NO | IRAS,[16] TPD[16] |
| | CO | IRAS,[16] TPD[16] |
| | $CH_3CHO$ | IRAS[253] |
| NbC(100) | $O_2$ | UPS[188] |
| | CO | UPS[188] |
| | $CH_3OH$ | UPS[188] |
| NbC(111) | $H_2/D_2$ | ARPES,[77] HREELS,[80] ICISS,[75] RHEED[75] |
| | $O_2$ | HREELS,[91] ICISS,[75] RHEED,[75] UPS[188] |
| | CO | ARPES,[119] UPS[188] |
| | $CH_3OH$ | UPS[188] |
| C/Ni/Pt(111) | $c$-$C_6H_{10}$ | HREELS,[163] TPD[58,163] |
| TaC(111) | $H_2$ | ARPES,[77] HREELS[80] |
| TiC(111) | $H_2$ | ARPES[21,79] |
| | $O_2$ | ARUPS,[97] DFT,[20] ICISS,[98] LEED,[97] STM,[88] XPS[97] |
| | CO | DFT[20,34] |
| | $CH_3OH$ | DFT,[20] UPS[74] |
| TiC(100) | $O_2$ | ARXPS,[84] DFT,[20,34] HREELS,[85] UPS,[34,84] XPS[85] |
| | $H_2O$ | AFM,[35] HREELS,[178,179] TPD[178,179] XPS[178] |
| | $NH_3$ | DFT,[34,224] HREELS,[224] TPD,[224] UPS[224] |
| | CO | DFT,[20,34,91,99] HREELS,[99] TPD,[99] UPS,[99] XPS[99] |
| | $CH_3OH$ | DFT,[20,183] HREELS,[183] TPD,[183] UPS,[74] XPS[183] |
| | $C_2H_5OH$ | HREELS,[193] TPD[193] |
| | $C_3H_7OH$ | TPD[193] |
| | $(CH_3O)_3PO$ | HREELS,[196] TPD,[196] XPS[196] |
| TiC(001) | $O_2$ | ISS,[96] STM,[87] UPS,[96] XPS[96] |
| | $SO_2$ | DFT,[220,221] SXPS,[220,221] TPD[220,221] |
| C/Ti(0001) | $O_2$ | AES[94] |
| | $CH_3OH$ | TPD,[185] HREELS[185] |
| | $C_2H_4$ | AES,[94] HREELS,[94] TPD[94] |
| | $C_6H_{10}$ | HREELS,[94] TPD[94] |
| $Ti_8C_{12}/Ti_{14}C_{13}$ | $SO_2$ | DFT[221] |
| VC(100) | $O_2$ | AFM,[86] DFT,[27] HREELS,[85] UPS,[34] XPS[85] |
| | $H_2O$ | TPD,[178] HREELS,[178] XPS,[178] AFM[35] |
| | $NH_3$ | DFT,[34,224] HREELS,[224] TPD,[224] UPS,[224] |
| | CO | DFT,[34,99] HREELS,[99] TPD,[99] UPS,[99] XPS[99] |
| | $CH_3OH$ | DFT,[183] HREELS,[183] TPD,[183] XPS[183] |
| | $C_2H_5OH$ | AFM,[194] HREELS,[193,194] STM,[194] TPD,[193,194] UPS,[194] XPS[194] |
| | $CF_3CH_2OH$ | AFM,[195] STM,[195] XPS[195] |
| | $C_3H_7OH$ | TPD[193] |
| | $(CH_3O)_3PO$ | HREELS,[196] XPS[196] |
| | $C_8H_{17}OH$ | AFM,[195] STM,[195] XPS[195] |
| C/V(110) | CO | HREELS[100,101] |
| | $CH_3OH$ | HREELS,[185] TPD[185] |
| | $C_2H_4$ | HREELS,[100,101] |
| | $C_4H_6$ | HREELS,[140] TPD[140] |
| | $C_4H_{10}$ | HREELS,[140] TPD[140] |
| | $c$-$C_6H_{10}$ | HREELS,[154] TPD[154] |
| WC(0001) | $O_2$ | ARUPS,[89] AES,[89] CLPES,[90] TPD[89] |
| | NO | ARUPS,[105,106] TPD[105] |
| | CO | ARUPS,[89,105,106] TPD[105] |
| | $C_2H_4$ | ARUPS,[106] |
| | $C_6H_6$ | ARUPS,[106,174] TPD[174] |
| WC(10$\bar{1}$0) | $O_2$ | HREELS,[91] UPS[91] |
| C/W(211) | $C_2H_2$ | HREELS,[130] TPD[130] |
| | $C_6H_6$ | HREELS[130] |
| C/W(111) | $H_2$ | TPD[81] |
| | $O_2$ | HREELS[95] |
| | $H_2O$ | HREELS,[110,111] TPD[110,111] |
| | NO | HREELS,[120,121] TPD,[120,121] SXPS[121] |
| | CO | HREELS,[110,111] TPD[110,111] |
| | $CH_3OH$ | HREELS,[81,110,189] TPD[81,110,189] |
| | $C_2H_4$ | HREELS,[128] TPD[128] |
| | $c$-$C_6H_{10}$ | HREELS,[95,155] NEXAFS,[155] TPD[95,155] |
| | $c$-$C_6H_{12}$ | HREELS[155] |
| C/W(110) | $H_2O$ | HREELS,[110,112] TPD[110,112] |
| | NO | TPD[120] |
| | CO | HREELS,[110,112] TPD[110,112] |
| | $CH_3OH$ | HREELS,[110,112] TPD[110,112] |
| | $C_2H_4$ | HREELS,[128] TPD[128] |
| | $C_6H_6$ | HREELS,[156] TPD[156] |
| | $c$-$C_6H_{10}$ | HREELS,[156] TPD[156] |
| C/W(100) | $O_2$ | LEED,[122] TPD[122] |
| | NO | TPD[122] |
| | $N_2$ | TPD[122] |
| | $N_2O$ | TPD[122] |
| | CO | HREELS,[118] NEXAFS[118] |
| | HCN | HREELS,[226] TPD,[225,226] XPS[226] |
| | $CH_2O$ | TPD[202] |
| | $CH_2O_2$ | TPD,[201] AES[201] |
| | $CH_3OH$ | TPD[192] |
| | $CH_3CN$ | HREELS,[228] TPD,[227,228] XPS[228] |
| | $C_2H_4$ | TPD[127] |
| | $C_2H_4O_2$ | TPD[203] |
| | $c$-$C_7H_8$ | TPD[168] |
| Pt/C/W(111) | $H_2$ | TPD[81] |
| | $H_2O$ | HREELS,[81] TPD[81] |
| | $CH_3OH$ | HREELS,[81,110] TPD[81,110] |
| | $c$-$C_6H_{10}$ | HREELS,[162] TPD[162] |
| WC/$W_2C$ film | CO | HREELS,[17] TPD[17] |
| | $CH_3OH$ | HREELS,[17] TPD[17] |
| ZrC(111) | $H_2$ | ARPES,[26,78] DFT,[63] HREELS[80] |
| | $O_2$ | ARPES,[23] UPS,[83] XAS,[32] XPS[83] |
| | CO | UPS[104] |
| | $CH_3OH$ | UPS[104] |
| ZrC(100) | $O_2$ | ARPES,[27] UPS,[83] XPS[82] |
| | $H_2O$ | ARPES,[181] UPS,[180,181] XPS[180,181] |
| | CO | UPS[104] |
| | $CH_3OH$ | UPS,[104,181] XPS[181] |

[a] 1-Butene. [b] Isobutene. [c] *cis*- and *trans*-2-butene.

have been utilized to investigate each of the chemical systems. Results from some of the earlier publications (before 1996) are not included in Table 2 and can be found in a previous review.[6]

## 3. Reactions with Diatomic Molecules

### 3.1. Hydrogen

The adsorption of hydrogen and deuterium has been investigated on the (111) surfaces of several groups 4 and 5 single-crystal carbides, TiC(111), ZrC(111), HfC(111), NbC(111), and TaC(111). Several surface techniques have been employed, including impact-collision ion-scattering spectroscopy (ICISS),[75,76] ARPES,[77−79] LEED,[76] reflection high-energy electron diffraction (RHEED),[75] and high-resolution electron energy loss spectroscopy (HREELS).[80] In all of these studies, the dissociative adsorption of hydrogen was observed at room temperature. ARPES results revealed the presence of a hydrogen-induced surface state on TiC(111)[21,79] and ZrC(111)[78] that was not detected on NbC(111)[77] and TaC(111),[77] suggesting that hydrogen was bonded to different sites on the groups 4 and 5 TMC surfaces. Ion-scattering studies indicated that deuterium adsorbed onto the threefold hollow site on the third layer metal atoms of both HfC(111)[76] and NbC(111).[75] HREEL spectra of hydrogen on ZrC(111), HfC(111), and NbC(111) revealed the $\nu$(metal-H) vibrational modes in the frequency range between 890 and 970 $cm^{-1}$,[80] consistent with the adsorption of atomic hydrogen on the twofold or threefold sites. These results correlated well with first principle calculations, which showed that hydrogen atoms preferentially occupied the ZrC(111) surface hollow sites in which the third layer Zr atoms were directly below the hydrogen.[63] On the other hand, HREELS measurements for hydrogen adsorbed on TaC(111) showed an unusually high-frequency feature at ~1680 $cm^{-1}$,[80] typically in the frequency range for atomic hydrogen on the terminal site. Overall, these studies indicate that hydrogen dissociates readily at room temperature on the groups 4 and 5 TMC surfaces. It appears that atomic hydrogen adsorbs in a similar environment on the three group 4 TMC surfaces, while the adsorption on the group 5 TaC(111) surface appears to be unique on the basis of the ARPES and HREELS measurements.

The reaction of hydrogen with carbide-modified group 6 surfaces, C/Mo(110)[61] and C/W(111),[81] has been investigated using TPD. The main motivation for these studies was to determine the feasibility of using group 6 carbides as potential electrocatalysts for hydrogen fuel cells. Hydrogen adsorbed dissociatively on the C/Mo(110) and C/W(111) surfaces at liquid nitrogen temperature and recombined to desorb as $H_2$ in a broad temperature range of 200−400 K. Analysis of the TPD results as a function of hydrogen exposure indicated a second-order desorption kinetics for atomic hydrogen from C/Mo(110).[61] More details about the theoretical modeling of the correlation between the electronic properties of C/Mo(110) and hydrogen binding energy will be discussed in section 8.

### 3.2. Oxygen

Oxygen adsorption has been extensively used as a prototype to demonstrate differences in the surface electronic structures of the (100) and (111) faces of groups 4 and 5 TMC surfaces. The reaction with oxygen often resulted in changes in the electronic states of TMC surfaces. For example, photoelectron spectroscopy measurements of oxygen adsorption on ZrC(100)[27,82] revealed that the formation of a ZrO-like layer altered the surface electronic structure, making the electronic properties of ZrO−ZrC(100) similar to those of ZrC(111).[23,83] Studies on oxygen-modified TiC(100) also indicated a similar increase of the density of states around the $E_F$ relative to the case of the unmodified surface.[84] Frantz and Didziulis reported XPS and HREELS results showing oxygen adsorbed dissociatively with preference for the carbon sites on TiC(100), eventually recombining with surface carbon to desorb as $CO_x$ species at higher temperatures.[85] DFT modeling using (100) $Ti_9C_9$ clusters also confirmed the preference in the formation of C−O over Ti−O surface bonds by over 50 kcal/mol.[34] On VC(100), however, oxygen dissociated to form a metastable overlayer of V=O species,[85] again consistent with DFT studies using (100) $V_9C_9$ clusters.[34] The difference in the adsorption sites of oxygen on these two (100) surfaces was attributed to the different electronic structures. For example, the highest occupied orbital in TiC is C 2p, leading to the bonding of oxygen on the carbon atom. In comparison, the one additional electron in the VC formula unit resides predominantly in a V 3d orbital, therefore favoring the formation of the V=O bond.

The effect of adsorbed oxygen on the frictional properties of VC(100) was also examined by Merrill and Perry using AFM.[86] Upon saturation adsorption of an oxygen adlayer, the coefficient of friction for VC(100) was reduced by nearly 40%. The observed change in friction was attributed to the decrease in the density of the metal d electrons near the Fermi level when the VC(100) surface was modified by oxygen.[86]

STM has been employed to compare the clean and oxygen-modified surfaces of TiC(001)[87] and TiC(111).[88] Kuramochi et al. showed that a defect-free (1 × 1) TiC(001) surface was inert toward the dissociation of oxygen.[87] When reconstructed to a $(\sqrt{2} \times \sqrt{2})$ structure, however, the surface became highly active toward oxygen dissociation, with oxygen adsorbing onto the carbon vacancies created by the surface reconstruction.[87]

The interaction of oxygen with WC(0001)[89,90] and WC(10$\bar{1}$0)[91] has been investigated using several techniques. TPD studies following the adsorption of $O_2$ on WC(0001) showed two recombinatory CO desorption peaks at ~750 and ~890 K.[89] Freund et al. attributed the first CO peak to the removal of surface carbon and the second to the reaction between oxygen and carbon in the second and subsequent layers. Angular-resolved UPS (ARUPS) further revealed the existence of WO, $WC_xO_y$, and elemental W at low temperatures. Oxidation at 1300 K resulted in the formation of a thin $WO_x$ surface layer.[89] Synchrotron-based CLPES investigations by Johans-

son and co-workers showed the W 4f components to be shifted and strongly attenuated upon relatively high oxygen exposures.[90] HREELS and UPS studies following room-temperature exposure of oxygen on WC(10$\bar{1}$0) were consistent with molecular adsorption; however, the O−O bond order was considerably reduced to a value between 1.05 and 1.25.[91]

The chemisorption of oxygen was studied on Mo- and C-terminated α-$Mo_2C$(0001) surfaces.[48,92] St Clair et al. found that on both surfaces CO was the only gas-phase product detected following oxygen adsorption, with the dominant CO desorption peak appearing at 834 K.[92] Quantitative analysis suggested that the reaction between adsorbed O and surface carbon to form CO was only a minority pathway (∼16%). The remaining 84% of the adsorbed oxygen diffused into the crystal bulk, which was consistent with studies of polycrystalline $Mo_2C$ powders.[92,93]

Results from the above studies clearly indicate that carbide surfaces are generally very active toward the dissociation of oxygen. The resulting oxygen-modified TMCs, often referred to as "oxycarbides" in the catalysis literature, should have chemical properties that are different from those of unmodified TMCs. Several studies have aimed at investigating the modification effect of oxygen on the chemical properties of C/Ti(0001),[94] C/Mo(110),[55] and C/W(111).[95] In these studies the carbide surfaces were exposed to $O_2$ at different temperatures to create different "oxycarbide" surfaces, which were subsequently investigated to determine the modification effect of oxygen on the chemical properties of TMC surfaces.[55,94,95]

For example, Figure 2 shows the HREELS results highlighting the different adsorption behavior of $O_2$ on C/Mo(110) at 600 and 900 K.[55] The peak at 386 $cm^{-1}$ was assigned to the $\nu$(Mo−C) mode, and the rest of the vibrational features were (Mo−O) vibrational modes of atomic oxygen occupying different surface sites. The oxygen binding environment was different on the 600 and 900 K O/C/Mo(110) surfaces, as indicated by the different $\nu$(Mo−O) frequencies on the two surfaces. For example, the HREEL spectrum of the 600 K O/C/Mo(110) surface strongly resembled that of the O/Mo(110) surface. As a consequence, the two O/C/Mo(110) surfaces were characterized by drastically different reactivities, with the 600 K O/C/Mo(110) surface being chemically inert and the 900 K surface remaining chemically active.[55]

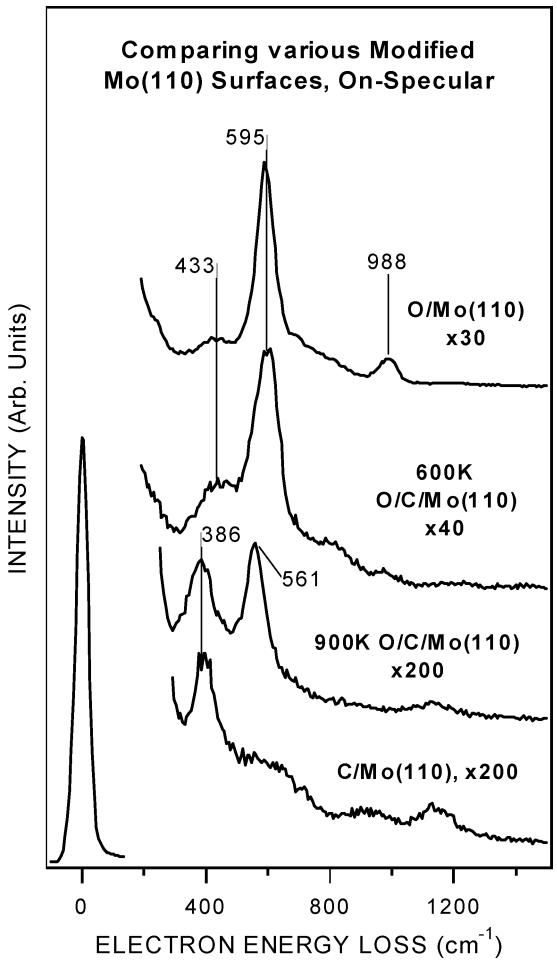


**Figure 2.** HREEL spectra comparing various chemically modified Mo(110) surfaces.[55] The C/Mo(110) surface was prepared by exposing clean Mo(110) to ethylene at 600 K followed by annealing to 1200 K to create the characteristic (4 × 4) LEED pattern. The 600 and 900 K O/C/Mo(110) surfaces were obtained after exposing the C/Mo(110) surface to 7 L of $O_2$ at 600 and 900 K, respectively.

## 3.3. Carbon Monoxide

The chemisorption and decomposition of CO on TMC surfaces have been extensively investigated to determine the relative electron accepting and donating capability of the substrate, as well as to illustrate the changes in reactivity upon carbide modification. Previous theoretical studies by Jansen and Hoffmann revealed a significant reduction in the ability of the TiC(100) substrate to donate electrons into the $2\pi^*$ antibonding orbitals of CO when compared with that of Ti(0001).[20] Experimentally, the adsorption of CO on TiC(100) was studied by Didziulis et al. using TPD, HREELS, UPS, and XPS.[99] The authors observed that a majority of the CO bonded weakly to the TiC(100) surface, as evidenced by a single desorption peak below 150 K. HREELS measurements did not show significant features attributable to CO adsorption until the spectra were taken with an ambient CO background. Heating to 180 K and above resulted in some CO decomposition, eventually leading to the formation of surface Ti=O species. On the basis of the UPS and XPS results, the authors concluded that the d−$2\pi^*$ interaction was nonexistent between TiC(100) and CO, which was supported by DFT calculations showing the metal atoms of the TiC terrace sites to be $d^0$ in character.[34,99] DFT results suggested that CO bonding with the carbon end down was more favored on the metal sites, with the adsorption energy nearly all provided through $\sigma$-donation.[34] The same study also compared the adsorption of CO on the TiC(111) surface, leading to the prediction that the adsorption energy of CO on TiC(111) would almost be twice that on TiC(100).[34]

The same authors also used the adsorption of CO as a probe to differentiate the electronic structures between VC and TiC.[34] The electronic structure of VC is different from that of TiC in part because of an additional electron in its formula unit.[99] Comparative studies showed that the heat of desorption

of CO was higher on VC(100) than on TiC(100). CO desorbed on VC(100) at ~200 K at low coverage and at 170 K for higher exposures. Low-temperature exposures of CO on VC(100) resulted in the detection of a $\nu$(C−O) mode at 2060 $cm^{-1}$. The authors suggested that the lower C−O stretching frequency observed on VC(100), as compared to 2120 $cm^{-1}$ on TiC(100), was indicative of greater d−2$\pi$* interaction. Additional photoemission measurements and DFT calculations also supported the conclusions that CO was bonded more strongly to VC(100) than to TiC(100), and that the surface metal atoms of VC behaved as $d^1$ species.[34]

The interaction of CO with carbide-modified V(110) surfaces, with atomic C/V ratios ranging from 0.1 to 0.4, has been examined by Chen and co-workers.[100,101] On all C/V(110) surfaces, CO molecules bonded to the terminal sites via the carbon end. TPD data revealed that CO desorbed molecularly from the surface at temperatures above 200 K. These observations were significantly different from that on clean V(110), where CO adsorbed in the parallel and inclined configurations characteristic of CO on other early transition metal surfaces.[102] Overall, the studies on the titanium and vanadium carbide surfaces agreed well with prior work suggesting that the formation of carbides reduced the degree of the interaction between the metal d band and the 2$\pi$* orbital of adsorbed CO.[103]

The adsorption of CO has also been employed to highlight the differences in the electronic structures of ZrC(100) and ZrC(111) surfaces.[104] CO adsorbed dissociatively on ZrC(111) and on oxygen-modified ZrC(100) at room temperature with a sticking probability near one. In contrast, CO adsorption was not observed on unmodified ZrC(100).[104] The difference in the surface reactivity toward CO was attributed to the participation of the electronic states around $E_F$ on ZrC(111) and oxidized ZrC(100); however, these surface states were not present on unmodified ZrC(100), leading to the weaker interaction of CO on ZrC(100).[23,27,82,104]

St. Clair et al. examined the interaction of CO on Mo-terminated and C-terminated α-$Mo_2C$(0001) surfaces.[92] Both surfaces exhibited similar activity toward CO, as indicated by the nearly identical molecular desorption temperature, decreasing from 440 to 345 K with increasing exposure. The only observable difference between the Mo- and C-terminated surfaces was the amount of CO uptake; the CO desorption area on the C-terminated surface was approximately 80% that on the Mo-terminated surface. Parallel UPS studies revealed an increase of 0.27 eV in the work function upon CO adsorption on α-$Mo_2C$(0001) at 300 K, suggesting some charge transfer due to the d−2$\pi$* back-bonding.[92]

Wang and co-workers studied the chemisorption of CO on a $\beta$-$Mo_2C$ foil with TPD and reflectance absorbance infrared spectroscopy (IRAS).[16] The recombinatory desorption of CO was detected near 1200 K, in addition to molecular desorption between 325 and 360 K. The high-temperature peak saturated at a very low coverage of CO even as the intensity of the low-temperature peak continued to increase. IRAS experiments comparing CO adsorption on $\beta$-$Mo_2C$ and the oxygen-modified $\beta$-$Mo_2C$ showed a vibrational mode at 2069 $cm^{-1}$ on both surfaces, though this feature appeared to be broader and less intense on the oxygen-modified surface. Furthermore, the preadsorption of oxygen also decreased the molecular desorption temperature of CO by approximately 50 K.[16]

The chemisorption of CO has also been studied on single-crystal WC(0001) using ARUPS.[105,106] The perpendicularly adsorbed CO molecules induced two valence bands at ~8.5 and ~11.5 eV, which were assigned to the 5$\sigma$/1$\pi$ and 4$\sigma$ states, respectively. Heating to 293 K resulted in these two features disappearing from the spectrum. The ARUPS spectrum at this temperature did not resemble that of a clean surface, but rather that of an oxygen-covered surface. Further heating to 878 K recovered the clean surface spectrum due to the recombinatory desorption of CO from the surface. Additional TPD measurements confirmed the ARPES results. Specifically, the authors detected two low-temperature molecular desorption states at 200 and 250 K, followed by a stronger CO peak centered at 720 K.[105] Brillo et al. also investigated the effect of preadsorbed oxygen on the adsorption of CO on WC(0001). At moderate oxygen coverages, CO chemisorption was essentially unaffected, as evident by the detection of the same 5$\sigma$/1$\pi$ and 4$\sigma$ ionization states. At higher oxygen coverages CO no longer adsorbed to the WC(0001) surface.[105,106]

Another important motivation for studying the interaction between CO and TMC surfaces is that the adsorption and desorption of CO play a critical role in the deactivation of electrocatalysts in hydrogen and methanol fuel cells.[107,108] The current anodic electrocatalysts, Pt/Ru alloys, are susceptible to CO poisoning due to the adsorption of CO under the fuel cell operating temperature, which is typically between 353 and 373 K.[109] Mo and W carbides have been suggested as a potential replacement for the Pt/Ru system, partially due to their higher tolerance to CO poisoning.[9−11] A series of fundamental studies using CO as a probe molecule was carried out on carbide-modified W(111),[110,111] W(110),[110,112] and Mo(110)[54] surfaces. On all three clean metal surfaces, CO readily decomposed; when heated to higher temperatures, the surface carbon and oxygen recombined to desorb as CO.[54,110−112] Upon carbide modification, however, the decomposition activity decreased to <10% of the adsorbed CO, with an overwhelming majority desorbing at or below 350 K. The presence of preadsorbed oxygen on the carbide surfaces also resulted in a significant reduction of the CO desorption temperature. For example, on C/W(111), CO desorbed at 330 and 355 K; with oxygen on the surface, however, CO desorbed at temperatures as low as 242 K.[110,111] The ability to desorb CO at lower temperatures would most likely translate into more resistance against CO poisoning. As compared in Table 3, the CO desorption temperatures on the carbide surfaces are significantly lower than those from the closed-packed Pt(111)[113,114] and Ru(0001)[115,116] surfaces, suggesting the possibility of carbides being

**Table 3. Comparison of CO Desorption Temperature from Carbide- and Oxycarbide-Modified Mo(110), W(110), and W(111), Pt, and Ru**

| surface | CO desorp temp[a] (K) |
|---|---|
| C/W(111)[110,111] | 330, 355 |
| 0.3 ML Pt/C/W(111)[81] | 357 |
| O/C/W(111)[110,111] | 242, 286 |
| C/W(110)[112] | 284, 335 |
| C/Mo(110)[182] | 336 |
| Pt(111)[113,114] | ~460 |
| Ru(0001)[115,116] | 400, 486 |
| Pt/Ru(0001)[116] | 325, 393, 459 |

[a] Desorption peak temperature.

more tolerant to CO poisoning in the temperature range 353−373 K.

### 3.4. Nitric Oxide

As a major component of the undesired $NO_x$ emission, the dissociation of NO has been the focus of several investigations to evaluate the potential of using carbides as an alternative De-$NO_x$ catalyst. The reaction of NO has been investigated on carbide-modified W(110),[120] W(111),[120,121] and Mo/W(111),[120] single-crystal WC(0001),[105,106] and polycrystalline $\beta$-$Mo_2C$ films.[16]

NO molecules adsorbed predominantly in an upright geometry on WC(0001) at 105 K, with some NO already dissociating at this temperature.[105,106] By 160 K, all adsorbed NO decomposed, and no low-temperature molecular desorption was detected even at near saturation coverage. Using ARUPS, Freund and co-workers observed features characteristic of an oxygen-covered surface when the overlayer was heated to above 500 K. TPD studies showed very little or no recombinatory NO desorption; however, atomic oxygen did react with surface carbon to desorb as CO at 720 and 860 K. Heating to above 900 K resulted in the recombinatory desorption of $N_2$.[105]

Wang et al. examined the chemisorption of NO on a $\beta$-$Mo_2C$ film using TPD and IRAS.[16] Low-temperature $N_2O$ and $N_2$ desorption features were observed, and recombinatory $N_2$ desorption peaks were recorded at 850 and 1100 K. In addition to a CO desorption feature at 1050 K, the authors also observed a weak CO signal at 350 K. Overall, their TPD results showed that NO underwent extensive decomposition and that the dissociation occurred for all exposures of NO up to saturation. IRAS measurements suggested that most of the NO molecules were strongly bonded to on-top sites and that some low-temperature dissociation of NO led to the availability of additional binding sites.[16]

Zhang and co-workers reported comparative studies of NO decomposition on carbide-modified W(111) and W(110) using TPD, HREELS, and SXPS.[120,121] $^{15}NO$ was used in the TPD experiments to differentiate $^{15}N_2$ (mass 30 amu) and CO (mass 28 amu) products. Both C/W(111) and C/W(110) readily decomposed NO. On C/W(111), low-temperature $N_2O$ and $N_2$ desorption states were detected at 167 K, with an additional high-temperature $N_2$ peak at 912 K. Coincidentally, CO desorption resulting from the reaction between oxygen and surface carbon was observed at the same temperature as $N_2$ desorption. The comparative investigation of the dissociation of NO on the open-structured C/W(111) and closed-packed C/W(110) surfaces also revealed the structure-dependent activity and product selectivity. The C/W(111) surface was more active toward NO decomposition and more selective toward the formation of the desirable De-$NO_x$ product ($N_2$) than C/W(110). At saturation NO exposure, the selectivity toward $N_2$ was 87% on the C/W(111) surface.[121] The C/W(110) surface, on the other hand, showed a selectivity of ~50% toward $N_2$ and $N_2O$.[120] Zhang et al. also demonstrated that oxygen modification on C/W(111) did not reduce either the decomposition activity toward NO or the high selectivity toward $N_2$.[121] In addition, alternating cycles of NO/hydrocarbon treatments successfully regenerated an active C/W(111) surface toward NO decomposition.[121]

As an extension of their studies on C/W(111), Zhang and co-workers also reported the decomposition of NO on carbide-modified Mo surfaces, where Mo was epitaxially grown on the W(111) substrate through physical vapor deposition.[120] In general, the interaction between NO and C/Mo/W(111) was similar to that on C/W(111) in terms of both dissociation activity and product selectivity, suggesting that the product selectivity of NO may be more sensitive to the substrate structure than to the identity of the parent metals.[120]

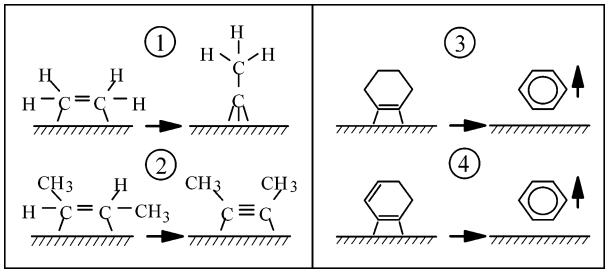


**Figure 3.** Schematics of characteristic hydrocarbon reaction pathways on Pt(111); see text for more detailed descriptions.

## 4. Reactions with Hydrocarbon Molecules

Hydrocarbons are the most frequently used probe molecules for studying the chemical properties of TMC surfaces. In particular, because the reaction pathways of hydrocarbons on Pt-group metal surfaces have been well established, the studies of carefully chosen hydrocarbon molecules provide insights into the presence or absence of Pt-like properties on the TMC surfaces. For example, Figure 3 shows several reaction pathways that are characteristic of the Pt(111) surface, including the conversion of ethylene to ethylidyne, the selective activation of the α-C−H bond of *cis*- and *trans*-2-butene to 2-butyne, and the selective dehydrogenation of cyclohexene and cyclohexadiene to benzene. As described below, these probe reactions have been studied on many TMC surfaces to determine whether they possessed the "Pt-like" chemical properties.

## 4.1. Linear Hydrocarbons

### *4.1.1. $C_1$ and $C_2$ Molecules*

The adsorption and decomposition of ethylene have been the focus of several experimental and theoretical investigations. Theoretical modeling of adsorbed ethylene on transition metals revealed that, for metals on the left side of the Periodic Table, a covalent bond was expected between ethylene and the metal.[123] On these early transition metal surfaces, the $\pi$ bond of ethylene was predicted to be effectively broken, leading to the formation of surface complexes containing a C−C single bond. This was in contrast to the case predicted for transition metals on the right side of the Periodic Table, where the bonding was more of a compromise between the covalent and donation−back-donation bonding configurations. Additional calculations indicated that the C−C bond order of adsorbed ethylene on late transition metals was likely to be between that of a double bond and that of a single bond.[123] Experimental studies generally confirmed the theoretical predictions of ethylene reactivity on various transition metal surfaces. On early transition metals, adsorbed ethylene underwent complete decomposition to yield atomic carbon and gas-phase hydrogen. In contrast, the reaction of ethylene often produced a stable ethylidyne ($CCH_3$) intermediate on the closed-packed surfaces of the Pt-group metals prior to complete dissociation at higher temperatures.[124] Because the ethylidyne intermediate is observed almost exclusively on Pt-group metal surfaces, the presence or absence of this surface species can be used to compare the similarities or differences between TMC and Pt surfaces.

Comparative investigations of the interaction of ethylene on clean and carbide-modified V(110),[101] Mo(100),[125] Mo(110),[126] W(100),[127] W(111),[128] W(110),[128] and Ti(0001)[94] surfaces have been reported. TPD measurements on these surfaces showed two similarities: (1) ethylene decomposed to produce atomic carbon and gas-phase hydrogen, and (2) the decomposition activity of the carbide surfaces toward ethylene was less than that of the clean surface, although the reduction in activity varies substantially from substrate to substrate. In addition to TPD experiments, HREELS studies have been instrumental in revealing the decomposition pathways of ethylene on the carbide surfaces. For example, Figure 4 compares the vibrational spectra of the surface intermediates after the reaction of ethylene on clean Ti(0001) and C/Ti(0001).[94] On the basis of comparisons with the existing literature of ethylene on other transition metal surfaces, the spectrum on the Ti(0001) surface can be readily assigned to di-$\sigma$ bonded ethylene as follows:[129] $\nu$(Ti−C) at 487 $cm^{-1}$, $\omega(CH_2)$ at 988 $cm^{-1}$, $\nu$(CC) at 1170 $cm^{-1}$, $\delta(CH_2)$ at 1394 $cm^{-1}$, and $\nu(CH_2)$ at 2916 $cm^{-1}$. In contrast, the 300 K spectrum of ethylene on C/Ti(0001) is significantly different from that on clean Ti(0001), particularly in the onset of doublet features in the $\delta$(CH) and $\nu$(CH) regions. As summarized in Table 4, all the vibrational modes on C/Ti(0001) can be assigned to the ethylidyne intermediate,[126,129] including the $\rho(CH_3)$ mode at 981 $cm^{-1}$, the $\delta_s(CH_3)$ and $\delta_{as}(CH_3)$ modes at 1373 and 1454 $cm^{-1}$, respectively, the $\nu$(C−C) mode at 1150 $cm^{-1}$, and the $\nu(CH_3)$ modes at 2882 and 2943 $cm^{-1}$.

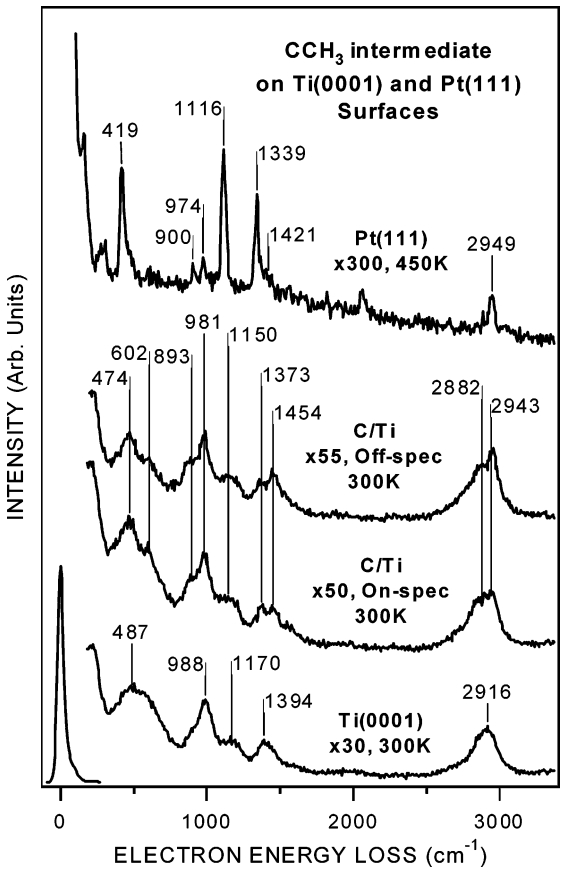


**Figure 4.** On- and off-specular HREEL spectra of ethylidyne following saturation exposures of ethylene at 100 K on C/Ti(0001)[94] and Pt(111), and heating to the indicated temperatures. The vibrational assignments are listed in Table 4.

The formation of the $CCH_3$ intermediate was also reported for several other closed-packed carbide-modified surfaces, including C/V(110),[101] C/Mo(110),[126] and C/W(110).[128] The characteristic vibrational frequencies of the ethylidyne intermediate on these surfaces are compared in Table 4. It is important to point out that the ethylidyne intermediate is not detected on the non-closed-packed substrates, such as C/Mo(100),[125] C/W(100),[127] and C/W(111).[128] This observation is consistent with studies of ethylene on Pt-group metals, where the formation of ethylidyne is typically detected only on the closed-packed surfaces.[124]

Although the ethylidyne intermediate is detected on both closed-packed TMC and Pt-group metal surfaces, there is a significant difference in the thermal stability. While ethylidyne species remain stable up to 400 K or higher on most Pt-group metal surfaces,[124] they start to decompose at 300 K or lower on carbide-modified surfaces.[94,101,126,128] Another noticeable difference is in the adsorption configuration of ethylidyne on the two types of surfaces. As compared in Figure 4, the detection of both the symmetric and asymmetric $CH_3$ deformation and stretching modes suggested that ethylidyne was adsorbed with the C−C bond in an inclined configuration with

**Table 4. Vibrational Frequencies of Ethylidyne on C/V(110), C/Mo(110), C/Ti(0001), C/W(110), and Pt(111)**

| mode | $(CH_3C)Co_3(CO)_9$[a] $((CD_3C)Co_3(CO)_9)$[129] | $C_2H_4(C_2D_4)$/ Pt(111) at 415 K[252] | $C_2H_4(C_2D_4)$/C/ V(110) at 150 K[101] | $C_2H_4$/C/ Ti(0001) at 300 K[94] | $C_2H_4(C_2D_4)$/C/ Mo(110) at 260 K[126] | $C_2H_4(C_2D_4)$/C/ W(110) at 200 K[128] |
|---|---|---|---|---|---|---|
| $\nu_s$(MC) | 401 (393) | 430 (410) | | 474 | 380 | 359 (379) |
| $\nu_{as}$(MC) | 555 (536) | 600 (600) | 600 (600) | 602 | 525 (560) | 663 |
| $\rho(CH_3)$ | 1004 (828) | 980 (790) | | 981 | 920 (670) | 879 (717) |
| $\nu$(CC) | 1163 (1182) | 1130 (1160) | 1095 (1080) | 1150 | 1075 (1105) | 994 (981) |
| $\delta_s(CH_3)$ | 1420 (1031) | 1350 (990) | 1385 | 1373 | 1345 (1015) | 1360 |
| $\delta_{as}(CH_3)$ | 1356 (993) | 1420 (1030) | | 1454 | 1430 | 1441 (1130) |
| $\nu_s(CH_3)$ | 2888 | 2890 (2080) | 2890 (2135) | 2882 | 2915 (2180) | 2929 (2178) |
| $\nu_{as}(CH_3)$ | 2930 (2192) | 2950 (2220) | | 2943 | | |

[a] $(CH_3C)Co_3(CO)_9$ frequencies from IR spectroscopy; $(CD_3C)Co_3(CO)_9$ frequencies from calculated results.

respect to the C/Ti(0001) surface; this was also consistent with the lack of angular dependence in the on- and off-specular HREELS measurements.[94] In contrast, the ethylidyne on Pt(111) showed only those vibrational modes with dynamic dipoles parallel to the C−C bond, consistent with ethylidyne being adsorbed with the C−C bond perpendicular to the Pt(111) surface.[129] It is very likely that the different thermal stability of ethylidyne is related to the different adsorption configuration, with the inclined ethylidyne being more susceptible to reactions with the surface and therefore starting to decompose at lower temperatures. Overall, the detection of ethylidyne suggests that the formation of carbide on early transition metals leads to the onset of the "Pt-like" properties. However, the differences in the thermal stability and adsorption orientation of ethylidyne also reveal that the chemical properties of the two types of surfaces are not identical. Similar conclusions can be drawn from the reactions of other probe molecules described later.

Acetylene is another $C_2$ molecule commonly used to probe the reactivity of carbide surfaces. Studies have been conducted on carbide-modified W(211)[130] to explore the possible cyclotrimerization of acetylene to benzene, which has been observed on Pd(111)[131−133] and Cu(110).[134,135] The use of the W(211) substrate also provided an example of carbide modification on a surface with highly corrugated structures. On both W(211) and C/W(211), acetylene decomposed to surface carbon and gas-phase hydrogen.[130] TPD results showed that, upon carbide modification, the hydrogen desorption feature shifted to higher temperatures and broadened significantly. Vibrational studies showed that acetylene interacted strongly with clean W(211) upon adsorption at 100 K to produce a variety of $C_2H_y$ intermediates, which decomposed completely by 700 K. On the other hand, acetylene remained intact and bonded to the C/W(211) surface in the $\sigma$-bonded configuration at 100 K. Heating the overlayer to higher temperatures resulted in the formation of stable intermediates with $CH_2$ or $CH_3$ groups, and the CH vibrations remained visible even at 700 K. This comparative study indicated that the surface reactivity of W(211) was significantly altered by the presence of interstitial carbon. In addition, the TPD and HREELS results did not show any evidence of acetylene cyclotrimerization on C/W(211).[130]

Solymosi and co-workers utilized halogenated hydrocarbons, such as $CH_3I$,[136] $CH_2I_2$,[137] and $C_2H_5I$,[137] to study the reaction of $C_xH_y$ species on a $Mo_2C$/Mo(111) surface. Compared to the Pt-group metals,[138,139] the $Mo_2C$/Mo(111) surface was less reactive toward C−I bond scission. Once the $CH_2$ species were formed following the dissociation of $CH_2I_2$, they underwent either self-hydrogenation to form methane or coupling to form ethylene on $Mo_2C$/Mo(111).[137] $C_2H_5I$ adsorbed molecularly on $Mo_2C$/Mo(111) at 100 K, with the C−I bond dissociating at temperatures above 150 K. Both gas-phase ethylene and ethane were detected from the surface reaction of adsorbed $C_2H_5$ species. The authors also reported that no $C_4$ or $C_1$ products were detected from the coupling of $C_2H_5$ or cleaving of the C−C bond. Additional vibrational spectra obtained for $CH_2I_2$ and $C_2H_5I$ on the $Mo_2C$/Mo(111) surface were consistent with the presence of di-$\sigma$ bonded ethylene at low temperatures and ethylidyne at higher temperatures.[137] Lastly, TPD results following the reaction of $CH_3I$ on $Mo_2C$/Mo(111) showed that methane, ethylene, and hydrogen were the gas-phase products.[136]

#### 4.1.2. $C_3$ and $C_4$ Molecules

Attempts to understand the activation of C−H bonds of *n*-butane have been carried out on C/V(110)[140] and C/Mo(110).[58] Although *n*-butane underwent reversible adsorption on clean V(110), the dissociation of *n*-butane was detected on the C/V(110) surface on the basis of the detection of the $H_2$ product in the TPD measurements. In contrast, the C/Mo(110) surface was essentially inert toward the dissociation of *n*-butane. The different activity of C/V(110) and C/Mo(100) toward *n*-butane was one of the first examples that clearly demonstrated that the reactivity of the carbide surfaces depended on the parent metals. In addition, the activation of the C−H bonds of *n*-butane on C/V(110) suggested that vanadium carbides might be a selective dehydrogenation catalyst, which was confirmed in the dehydrogenation of *n*-butane on polycrystalline VC powder catalysts.[141]

Reactions of 1-butene and isobutene on clean and carbide-modified Mo(110) have been investigated using HREELS.[142] On clean Mo(110), isobutene dehydrogenated to produce $C_xH_y$ fragments. In contrast, the reaction pathway of isobutene on C/Mo(110) led to the formation of the isobutylidyne intermediate, which resembled that observed on Pt(111)[143] and Ru(0001).[144] Further heating resulted in C−C bond scission of the isobutylidyne species to form surface methyl groups.[142] Results on the activation sequence of C−H and C−C bonds of isobutene suggested that C/Mo(110) may be better suited for hydrogenolysis

reactions because of its ability to selectively cleave the C−C bonds. Similar conclusions were derived on the basis of the reaction mechanisms of 1-butene on C/Mo(110).[142]

As depicted earlier in Figure 3, the selective activation of the α-CH bonds of 2-butenes is a characteristic surface reaction on Pt(111).[143] Vibrational studies monitoring the reaction pathways of *cis*- and *trans*-2-butenes on Mo(110) and C/Mo(110) were used as probe reactions to study the potential "Pt-like" activity.[145] The clean Mo(110) surface was nonselective toward the dissociation of the α- and β-CH bonds, in particular in the dissociation of the *trans*-2-butene. In contrast, the C/Mo(110) surface led to the selective α(C−H) bond cleavage for both 2-butenes to produce 2-butyne. This study provided another important example of converting the activity of Mo(110) to "Pt-like" via the formation of surface carbide.[145]

The adsorption and surface reactions of propyl iodide ($C_3H_7I$)[146] and allyl iodide ($C_3H_5I$)[147] on $Mo_2C$/Mo(100) surfaces have been investigated by Solymosi et al. using TPD, XPS, and HREELS. After the scission of the C−I bond, $C_3H_7$ fragments underwent predominantly dehydrogenation and hydrogenation at ~300 K to produce gas-phase propene and propane, respectively.[146] At higher temperatures, hexane and hexene products, resulting from coupling reactions, were also detected in TPD measurements. HREELS analysis of the $C_3H_7I/Mo_2C$/Mo(100) overlayer suggested the formation of di-σ bonded propylene at 200 K, which then converted to propylidyne at ~300 K.[146] Studies of allyl iodide on $Mo_2C$/Mo(100) led to similar conclusions. Allyl iodide also resulted in the production of gas-phase propene and propane, as well as the coupling products, hexane and hexadiene.[147] One significant difference between the chemistry of $C_3H_7I$ and $C_3H_5I$ was that the coupling products from the $C_3H_5$ desorbed before the hydrogenated products (propene and propane), whereas the coupling products of $C_3H_7$ desorbed after propene and propane.[146,147]

## 4.2. Cyclic Hydrocarbons

The selective dehydrogenation of cyclohexene to produce gas-phase benzene is another probe reaction often used to demonstrate the similarities in the surface reactivity between carbide and Pt-group metal surfaces. For example, on Pt(111), the only desorption products detected following the reaction of cyclohexene adsorption were $H_2$ and benzene.[148,149] Vibrational studies have revealed that adsorbed cyclohexene molecules were completely converted to adsorbed benzene on Pt(111) at 300 K.[148−150] Although the selectivity for converting cyclohexene to surface benzene was nearly 100% at 300 K, a significant fraction of surface benzene underwent subsequent thermal dissociation instead of desorbing to the gas-phase. Rodriguez and Campbell reported that the selectivity toward the production of gas-phase benzene depended on the initial surface coverage of cyclohexene on Pt(111).[151]

Comparative HREELS and TPD studies of cyclohexene on clean and carbide-modified Mo(110) surfaces[152,153] showed that the formation of carbide significantly enhanced the dehydrogenation selectivity. For example, on clean Mo(110), cyclohexene adsorbed irreversibly and underwent complete decomposition without producing surface or gas-phase benzene. On C/Mo(110), however, cyclohexene primarily underwent partial dehydrogenation, with a ~70% selectivity toward the production of gas-phase benzene. Moreover, HREELS measurements on C/Mo(110) did not detect benzene as a surface intermediate, indicating that the evolution of gas-phase benzene was a reaction-limited process[152,153] instead of the desorption-limited process on Pt(111).[148−151] The difference in the desorption temperature of the benzene product is illustrated in Figure 4, which compares the TPD spectra of benzene from the dehydrogenation of cyclohexene on Pt(111) and on several carbide-modified surfaces.

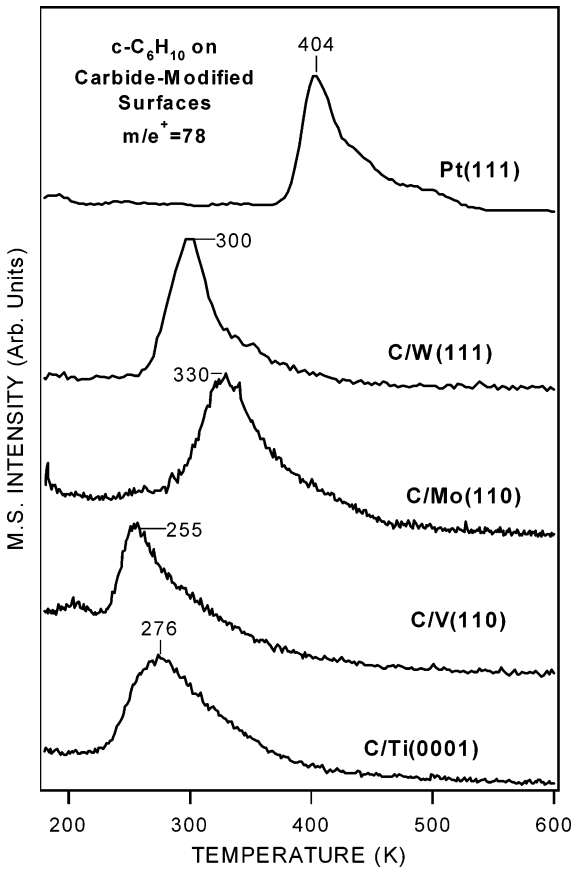


**Figure 5.** TPD spectra of benzene (mass 78) obtained following saturation exposures of cyclohexene (*c*-$C_6H_{10}$) on C/Ti(0001),[94] C/V(110),[154] C/Mo(110),[152] C/W(111),[155] and Pt(111).[150] A linear heating rate of 3 K/s was used in all TPD experiments.

As compared in Figure 5, the selective dehydrogenation of cyclohexene was also observed on other carbide-modified surfaces, including C/Ti(0001),[94] C/V(110),[154] and C/W(111).[155] Similar to the case observed on clean Mo(110), benzene is not produced on the clean surfaces of Ti(0001), V(110), or W(111). The formation of carbide on these surfaces introduced the dehydrogenation reaction pathway, resulting in the production of gas-phase benzene. Similar to the case on C/Mo(110), corresponding HREELS measurements did not detect the surface benzene intermediate on other carbide-modified surfaces,[94,154,155] indi-

**Table 5. Benzene Selectivity from C/Ti(0001), C/Mo(110), C/W(111), and Corresponding Oxycarbide Surfaces**

| surface | $C_6H_6$ activity: cyclohexene per metal atom (% selectivity) | complete decomposition activity: cyclohexene per metal atom (% selectivity) | overall activity: cyclohexene per metal atom |
|---|---|---|---|
| 750 K C/Ti(0001)[94] | 0.084 (50) | 0.084 (50) | 0.168 |
| 850 K C/Ti(0001)[94] | 0.134 (69) | 0.059 (31) | 0.193 |
| 750 K O/C/Ti(0001)[94] | 0.139 (90) | 0.015 (10) | 0.154 |
| C/Mo(110)[152,153] | 0.035 (70) | 0.015 (30) | 0.050 |
| 900 K O/C/Mo(110)[55] | 0.014 (39) | 0.022 (61) | 0.036 |
| C/W(111)[155] | 0.059 (67) | 0.029 (33) | 0.088 |
| 900 K O/C/W(111)[95] | 0.054 (83) | 0.011 (17) | 0.065 |
| 0.5 ML Pt/C/W(111)[162] | 0.076 (86) | 0.012 (14) | 0.088 |
| Pt(111)[148−151] | 0.120 (100)[a] | 0.090 (75)[a] | 0.120 |

[a] All adsorbed cyclohexene was converted to surface benzene, of which ~25% subsequently desorbed as gas-phase benzene.

cating that the desorption of benzene is also a reaction-limited process. It is also interesting to point out that the desorption temperature of the benzene product from the four carbide-modified surfaces is in the range 255−330 K, significantly lower than the desorption temperature from Pt(111). The activity and selectivity to gas-phase benzene on the carbide-modified surfaces are summarized in Table 5. In brief, the values presented in Table 5 were derived by first correlating the carbon signal from AES to the hydrogen desorption peak area from TPD on the clean metal surfaces, on which only the complete decomposition of cyclohexene was observed ($m\cdot c\text{-}C_6H_{10} \rightarrow 6m\cdot C + 5m\cdot H_2$). By comparing the $H_2$ desorption peak area on carbide surfaces relative to the clean surface, one can then obtain the percentage of hydrogen desorption attributable to benzene formation ($n\cdot c\text{-}C_6H_{10} \rightarrow n\cdot C_6H_6 + 2n\cdot H_2$). Lastly, the summary in Table 5 does not include reversible molecular desorption as a reaction pathway.

Cyclohexene has been used as a probe molecule to differentiate the surface activity of C/W(111)[155] and C/W(110).[156] In general, the reaction pathways of cyclohexene on C/W(111)[155] were similar to those on C/Mo(110).[152,153] Gas-phase benzene desorbed from C/W(111) at 300 K at ~67% selectivity. Parallel studies on the C/W(110) surface illustrated the substrate-dependent reaction pathways of cyclohexene.[156] While the C/W(110) surface was still active toward the decomposition of cyclohexene, it was unlike either C/W(111) or C/Mo(110) in that only between 7 and 18% of the adsorbed cyclohexene dehydrogenated to produce benzene. A possible explanation for the differences in product distribution between C/W(110) and C/W(111) may involve the location of the carbon atoms. In these comparative studies, both C/W(111) and C/W(110) were annealed to 1200 K to produce the carbide-modified surfaces. The (111) plane of tungsten has an open-structured surface, which would allow the carbon atoms to situate between the metal atoms. Since W(110) is a closed-packed surface, carbon would most likely act as site-blockers on top of metal atoms. Furthermore, one would expect the surface reactivity of C/W(110) and C/Mo(110) to be relatively similar, since both W and Mo are group 6 metals with an identical crystal structure and similar atomic radius.[156] The observed differences between the two surfaces were related to the temperatures that were required to induce the inward diffusion of surface carbon. Thermal studies have shown that C/Mo(110) did not exhibit "Pt-like" reactivity until the surface was annealed to 1200 K.[152,153] The importance of the annealing process was that some of the surface carbon atoms diffused into interstitial sites, enabling surface Mo atoms to react with cyclohexene. Previous AES experiments, however, have shown that carbon did not diffuse inward on W(110) until above 1531 K.[157] As a result, the C/W(110) surface after annealing to 1200 K did not possess the "Pt-like" dehydrogenation selectivity due to the site-blocking by surface carbon on W(110).[156]

The reaction of cyclohexene has also been utilized as a probe to determine the effect of oxygen modification on the reactivity of C/W(111),[95] C/Mo(110),[55] and C/Ti(0001)[94] using TPD and HREELS. The motivation to undertake this study was due to the fact that during catalytic processes the surfaces of TMCs are often oxidized by air or by oxygen-containing reactants and products, leading to the formation of the so-called "oxycarbide". Several research groups have reported that the catalytic properties of powder carbides can be significantly modified by the presence of oxygen.[158−161] As discussed earlier in Figure 2, the adsorption of oxygen on C/Mo(110) at 600 and 900 K led to oxygen residing in different bonding environments,[55] which was also confirmed in the dissociation of oxygen on C/W(111) at 600 and 900 K.[95] Correspondingly, thermal desorption studies following cyclohexene adsorption on the 600 K O/C/Mo(110) and O/C/W(111) surfaces showed only reversible molecular desorption. In contrast, oxygen modification at 900 K resulted in oxygen occupying either the twofold, threefold, or interstitial sites, but not the terminal on-top sites. AES measurements also revealed a reduction in the atomic C/W ratio after oxygen modification at 900 K. These results suggested that surface carbon was removed by oxygen via the formation of gas-phase CO at 900 K, and subsequently some oxygen occupied the sites left vacant by carbon. For example, quantitative analysis (Table 5) showed that, on the 900 K O/C/W(111) surface, ~83% of the cyclohexene dehydrogenated to yield gas-phase benzene, which was higher than the ~67% selectivity observed on unmodified C/W(111).[95]

The dehydrogenation of cyclohexene has also been investigated on Pt-modified C/W(111) surfaces.[162] The motivation for supporting submonolayer Pt onto the C/W(111) surface was to determine the feasibility of using carbide as a catalytic support. Studies comparing the reactivity of Pt-modified C/W(111) with those

of clean C/W(111) and Pt(111) demonstrated an enhancement toward the production of benzene from cyclohexene. On submonolayer Pt-modified C/W(111), the selectivity toward gas-phase benzene formation was at ~86%,[162] which was higher than that on either Pt(111) (25%)[148,149,151] or C/W(111) (67%).[155] One possible explanation for the enhancement toward benzene production was that the energy barrier for benzene desorption was reduced on Pt/C/W(111) relative to the Pt(111) surface.[162] This assertion was supported by the observation that benzene desorption was reaction-limited at 290 K on Pt/C/W(111)[162] but desorption-limited at ~400 K on Pt(111).[148,149,151] The lower barrier for benzene desorption prevented the subsequent thermal decomposition of the surface benzene intermediate, leading to a higher selectivity toward gas-phase benzene.[162]

Cyclohexene has also been used as a probe to study the effect of carbide modification on Ni,[163] a late transition metal. An epitaxial Ni thin film was prepared by depositing Ni atoms onto a Pt(111) surface until Pt signals were no longer detectable within the Auger probing depth. LEED experiments verified the Ni/Pt(111) surface to be essentially a Ni(111) film.[150,163] A carbon overlayer similar to those described for early transition metals was then prepared by decomposing ethylene or cyclohexene. Alternatively, carbide layers can also be grown on a Ni surface by the Boudouard reaction, $2CO(g) \rightarrow C(ads) + CO_2(g)$.[164,165] Unlike those on early transition metals, the carbon overlayer on Ni was carbidic at 600 K but changed to graphitic when heated to 900 K. On both carbide- and graphite-modified Ni surfaces, benzene desorption was observed following cyclohexene dehydrogenation; however, the overall activity toward cyclohexene was reduced by a factor of 2.2 upon graphite formation. HREELS results further demonstrated that the surface benzene intermediate was bonded differently onto carbide- and graphite-modified Ni surfaces.[163] Additional studies on other late transition metal carbide surfaces may help identify general similarities and differences between the surface reactivities of early and late transition metal carbides.

Reactions of TMC surfaces with other cyclic molecules, such as cyclopropane,[166] cyclopentene,[53] cyclohexane,[167] cyclohexadiene,[153] and cycloheptatriene,[168] have also been investigated. For example, the thermal behavior of 1,3-cyclohexadiene on the C/Mo(110) surface was similar to that observed for cyclohexene.[153] On clean Mo(110), 1,3-cyclohexadiene primarily underwent complete decomposition, with only trace amounts of gas-phase benzene detected over a broad temperature range between 200 and 400 K. On C/Mo(110), however, a benzene desorption peak was observed at 313 K. Detailed vibrational studies revealed additional differences in the decomposition pathways of cyclohexadiene on the two surfaces. Following adsorption at 80 K on clean Mo(110), cyclohexadiene immediately dehydrogenated to form benzene. Heating to 300 K resulted in an HREEL spectrum consistent with the presence of a benzyne ($C_6H_4$) intermediate. On the other hand, surface benzene species were not observed on the C/Mo(110) surface upon cyclohexadiene adsorption. By 300 K, the HREEL spectrum appeared to resemble that of a phenyl intermediate.[153]

## 4.3. Aromatics

There has been an abundance of literature detailing the adsorption of benzene on transition metal surfaces.[169−171] These studies revealed that benzene typically adsorbed with the molecular plane nearly parallel to the substrate at low coverages and that the out-of-plane C−H bending mode ($\nu_4$ according to the Herzberg notation) of adsorbed benzene correlated with the strength of the benzene−metal interaction. Studies on clean and carbide-modified Mo(110) showed that benzene also adsorbed with the molecular plane parallel to the surface;[172] however, the approximately linear correlation between the vibrational frequency of the $\nu_4$ mode and the cohesive energy of the metal substrate could not be extended to include the C/Mo(110) surface. Furthermore, the comparative study also revealed different decomposition mechanisms for benzene on the two surfaces. On clean Mo(110), chemisorbed benzene remained stable until ~325 K, above which it decomposed to a benzyne intermediate. In contrast, $C_2H$ and CH fragments were produced on the C/Mo(110) surface upon heating to 470 K. The latter decomposition pathway was similar to that observed on Rh(111),[173] providing another example of similar activity between C/Mo(110) and Pt-group metal surfaces.

The adsorption of benzene on clean and carbide-modified W(211) was examined as part of the acetylene cyclotrimerization studies.[130] Benzene did not bond with the molecular plane parallel to the clean W(211) surface, as evidenced by the presence of an intense $\nu$(C−H) mode at 3051 $cm^{-1}$ and the lack of a strong angular dependence for all benzene vibrations. These HREELS results were consistent with a tilted adsorption geometry for benzene, which may be attributed to the row-and-trough structure of clean W(211). Interestingly, the presence of carbon atoms on the C/W(211) surface appeared to "smooth" the surface, which led to the adsorption of benzene in the parallel adsorption geometry on C/W(211).[130] More studies are needed to determine whether the "smoothing" behavior is due to an electronic modification or a physical reconstruction of the corrugated W(211) surface.

ARPES studies of benzene on WC(0001) have been reported by Brillo and co-workers.[106,174] Evidence of benzene decomposition on clean WC(0001) was observed at 210 K. The photoemission spectrum of the surface intermediate at this temperature was virtually identical to that obtained following ethylene decomposition on WC(0001). At temperatures above 300 K, the $C_xH_y$ fragments further dehydrated to produce surface carbon. Additional studies on oxygen-modified WC(0001) showed a reduced strength of the benzene−substrate interaction with increasing oxygen coverage.[106,174]

The adsorption and decomposition of phenyl iodide ($C_6H_5I$) over the $Mo_2C$/Mo(100) surface were investigated by Solymosi and co-workers using TPD, XPS, and HREELS.[175] At 100 K and at submonolayer

coverages, phenyl iodide adsorbed molecularly with the aromatic ring parallel to the surface. The scission of the C−I bond occurred between 162 and 300 K, resulting in the formation of surface phenyl species. The majority of the phenyl species hydrogenated to form gas-phase benzene at ~290 K. The remaining surface species further dehydrogenated to produce benzyne, followed by additional dehydrogenation steps leading to hydrogen desorption at 600 K and above. The photolysis of the $C_6H_5I$ layer on $Mo_2C$/Mo(100) by UV light was also investigated, which led to the C−I bond scission at temperatures as low as 100 K.[175]

## 5. Reactions with Oxygen-Containing Molecules

### 5.1. Water

A detailed understanding of the reaction of water on carbide surfaces is of practical significance in two areas, tribology[176,177] and fuel cells.[110−112] Investigations into the chemical reactivity of TiC and VC surfaces with respect to their use as coatings in tribological applications have been reported recently.[178,179] Perry and co-workers observed four molecular desorption states of deuterated water at 188, 233, 263, and 308 K on TiC(100) at saturation exposure.[179] XPS studies showed the formation of three adsorbed species at low temperatures: atomic O, partially dissociated hydroxyl groups, and molecular water.[178] Heating the surface resulted in the desorption of $D_2$, CO, and $CO_2$ species. The desorption peaks of CO and $CO_2$ spanned across a wide temperature range from 173 to 773 K, while the $D_2$ desorption peak was relatively weak and was detected at ~500 K. HREEL spectra obtained following the adsorption of $D_2O$ on TiC(100) showed evidence of some O−D bond dissociation at 144 K. The authors also assigned the vibrational modes at 710 and ~2100 $cm^{-1}$ to the stretching modes of Ti−D and TiC−D, respectively, which were consistent with the dissociative adsorption of $D_2O$. Spectral changes upon heating to higher temperatures included the disappearance of molecular features and an increase in the intensity of the Ti=O stretch at 980 $cm^{-1}$.[178,179]

Studies comparing the reaction of water on TiC(100) and VC(100) led to the conclusion that the low-temperature decomposition was more extensive on TiC(100).[178] Similar to the case on the TiC(100) surface, TPD experiments also revealed four molecular desorption states on VC(100) at 175, 202, 243, and 283 K. A major difference between the two surfaces was that molecular desorption occurred mainly above 200 K on TiC(100) but below 200 K on VC(100). TPD studies showed the evolution of gas-phase hydrogen and the formation of stable V=O species between 300 and 400 K. Unlike the case on TiC(100), carbon from the VC(100) substrate did not react with adsorbed water or hydroxyls to produce gas-phase CO and $CO_2$.[178] These studies could provide insights into the interaction between coating materials and their respective lubricants. For example, the ability of VC to form a stable V=O may be an attractive characteristic for applications requiring oxygen-resistant coatings.[178]

XPS and UPS studies of the reactivity of water on the ZrC(100) surface have been reported by Edamoto and co-workers.[180,181] As described earlier, these authors showed that the (100) plane of ZrC was inactive toward CO and hydrogen as a result of a relatively small DOS around $E_F$.[104] Similarly, water did not adsorb on ZrC(100) at room temperature; however, when a well-ordered suboxide-like layer was formed on ZrC(100), the surface became significantly more active toward water dissociation.[180,181] Furthermore, XPS and UPS measurements provided evidence supporting the dissociative adsorption of water at room temperature to form atomic oxygen and surface hydroxyl species.

The ability of carbide surfaces to decompose water is important in direct methanol fuel cell (DMFC) applications. Specifically, water dissociates to produce surface hydroxyl groups, which then react with adsorbed CO to desorb as $CO_2$.[107,108] This is a critical reaction in DMFCs because it removes the CO surface intermediate from poisoning the fuel cell electrocatalyst and it generates two of the six electrons in the overall electrooxidation of a methanol molecule.[107,108] To determine the feasibility of using tungsten carbides as potential electrocatalysts in DMFCs, the reaction of water has been studied on carbide-modified W(111)[110,111] and W(110).[110,112] On the clean W(111) and W(110) surfaces, decomposition of water was apparent even at liquid nitrogen temperature, as evident by the formation of surface OH species. Heating the adsorbed layer resulted in the desorption of hydrogen and the accumulation of atomic oxygen on the surface. Quantitative calculations showed a decomposition activity of 0.32 water molecules per W atom on both surfaces. On the carbide-modified surfaces, both substrates showed a reduction of ~50% in the activity toward water dissociation. The TPD measurements also revealed differences in both the hydrogen desorption peak shape and temperature from C/W(111) and C/W(110). The corresponding HREEL spectra monitoring the decomposition of water on C/W(110) showed only a very weak $\nu$(OH) mode while the same mode on C/W(111) was relatively prominent. The combined analysis of HREELS and TPD results suggested that the evolution of gas-phase hydrogen was reaction-limited on C/W(111) but desorption-limited on C/W(110),[110−112] indicating the structure dependence of the dissociation of water on the tungsten carbide surfaces.

Coadsorption experiments of CO and $H_2O$ were also conducted on C/W(111) and C/W(110) to determine whether the formation of $CO_2$ occurred under UHV conditions.[111,112] Although the presence of surface hydroxyls led to a decrease in the CO desorption temperatures, the TPD and HREELS experiments did not detect the desorption of $CO_2$ or the formation of surface $CO_2$ intermediates.

The interaction between water and C/Mo(110)[182] was carried out as an extension to the studies on C/W(111) and C/W(110). The surface science work was motivated by the electrochemical studies of Kudo et al.,[9−11] who incorporated molybdenum carbides into tungsten carbides as a promoter in DMFC systems. The presence of Mo carbides was suggested

either to aid in the removal of surface poisons or to alter the reaction pathways leading to the inhibition of poisonous species.[9−11] Using identical experimental conditions to those for C/W(111) and C/W(110), the TPD results showed the decomposition activity on the Mo(110) substrate to be less affected by carbide modification than that on the tungsten surfaces.[182] Specifically, the decomposition activity of water on C/Mo(110) was approximately 73% of that on the Mo(110) surface; this was in contrast to the ~50% value on the C/W surfaces.[110−112] The enhanced ability of the C/Mo(110) surface to dissociate water, relative to that on C/W(111) and C/W(110) surfaces, could possibly promote the removal of CO adsorbed on the electrocatalyst surface.[182]

## 5.2. Alcohols

The reactions of methanol on transition metal and metal oxide surfaces have been investigated extensively.[138,139] One of the underlying motivations for these studies was to understand the mechanisms of the Fischer−Tropsch reaction.[183,184] These studies have provided a significant reference base to compare the reaction pathways of methanol on TMCs with those of the corresponding metal and metal oxide surfaces.

The adsorption and reaction of methanol on TiC(100) have been investigated using HREELS, XPS, and TPD.[183] $CH_3OH$ adsorbed dissociatively to form methoxy on the TiC(100) surface at temperatures as low as 153 K, as suggested by the absence of the $\nu$(O−H) vibrational mode of molecular methanol. As the surface temperature increased from 190 to 300 K, the methoxy species recombined with hydrogen to desorb as methanol. At temperatures above 300 K, small amounts of gas-phase hydrogen and methane were observed from the surface, which were attributed to the decomposition of methanol at defect sites. Comparative studies were conducted on VC(100) to examine the effect of substrate electronic structure on the decomposition of methanol.[183] As mentioned earlier, VC(100) possesses an additional 3d valence electron per formula unit when compared to TiC(100). HREELS results following methanol adsorption on VC(100) showed that, at low temperatures, the scission of the O−H bond to form methoxy was less extensive than that on TiC(100). When samples were heated to higher temperatures, recombinative methanol desorption was observed between 300 and 500 K. Unlike that on TiC(100), however, a significant percentage of adsorbed methoxy underwent further decomposition to yield gas-phase formaldehyde and hydrogen, along with a small amount of methane and surface oxygen. The authors attributed the formation of formaldehyde from VC(100) to the interaction between the methyl group of methoxy and the surface metal states.[183]

To compare carbide-modified surfaces with bulk carbide single crystals, Zellner et al. investigated the reaction of methanol on carbide-modified Ti(0001) and V(110) surfaces.[185] There were general similarities between the carbide-modified surfaces and the corresponding bulk crystals in terms of the methanol reaction pathways. For example, the dissociation of methanol to methoxy was observed on C/Ti(0001) at liquid nitrogen temperature, with most of the methoxy species recombining with surface hydrogen to desorb as methanol at higher temperatures. In contrast, a significant fraction of methanol adsorbed on C/V(110) without the scission of the O−H bond at liquid nitrogen temperature, although all the surface methoxy species underwent complete decomposition at higher temperatures without desorbing as methanol. These reaction pathways were very similar to those on bulk TiC(100) and VC(100) surfaces[183] described in the previous paragraph; however, the C/Ti(0001) and C/V(110) surfaces appeared to be much more reactive than the TiC(100) and VC(100) surfaces in terms of the fraction of methanol that underwent complete decomposition.[183,185] This is likely due to the fact that the Ti(0001) (hcp structure) and V(110) (bcc structure) substrates have the sixfold or quasi-sixfold symmetry. The corresponding C/Ti(0001) and C/V(110) surfaces will therefore resemble the sixfold symmetry of the (111) surfaces of TiC and VC, which should be more active than the corresponding (100) surfaces.[183,185]

Edamoto and co-workers conducted UPS measurements following methanol adsorption on TiC(100) and TiC(111) surfaces at room temperature.[74] The authors chose to expose 200 L (langmuirs) of methanol on TiC(100) but only 5 L on TiC(111). The decision to use different exposures probably stemmed from a lower sticking probability of methanol on TiC(100). UPS data following the adsorption of methanol on TiC(100) showed features that could be ascribed to the 2a″, 7a′, 6a′ + 1a″, and 5a′ orbitals, which indicated the presence of molecularly adsorbed methanol.[186] The seemingly contradictory conclusions of methanol on $CH_3OH$ reported by Edamoto et al. and Franz et al. may have been caused by the differences in methanol exposure and in the adsorption temperature.[74,183] In contrast, room-temperature adsorption on TiC(111) resulted in the appearance of two features at 5.5 (2e orbital) and 9.2 (1e + $5a_1$ orbitals) eV, which were attributed to the formation of the methoxy intermediate.[74,187] Edamoto and co-workers also considered the 5.5 eV feature to include emissions from atomic O, H, and C resulting from the complete decomposition of methanol.[74]

Studies of methanol adsorbed on ZrC(111)[104] revealed nearly identical results to those on TiC(111).[74] Room-temperature adsorption of methanol on ZrC(111) induced two UPS features at 6.0 and 10.0 eV, again indicative of the presence of methoxy.[187] On the basis of work function calculations and by comparing with previous adsorption studies with $O_2$, $H_2$, and CO, Edamoto and co-workers suggested that the complete decomposition pathway dominated in the initial stages of methanol adsorption.[104] Once the surface was covered with atomic C, H, and O species, however, the methoxy intermediate began to accumulate. As was the case on TiC(100),[74] methanol adsorbed molecularly on ZrC(100) at room temperature.[104,181] When the ZrC(100) surface was modified by oxygen to form a ZrO-like layer, however, methanol was observed to adsorb dissociatively, resulting in UPS features indicative of methoxy. These results

**Table 6. Comparison of Activity and Selectivity of $CH_3OH$ on C/Ti(0001), C/V(110), C/Mo(110), C/W(111), and C/W(110)**

| surface | complete decomposition activity per metal atom (%) | CO activity per metal atom (%) | $CH_4$ activity per metal atom (%) | recombinatory $CH_3OH$ desoprtion |
|---|---|---|---|---|
| Mo(110)[182] | 0.260 (84) | 0.048 (16) | 0 | 0 |
| C/Mo(110)[182] | 0.142 (63) | 0.083 (37) | 0 | 0 |
| W(110)[112] | 0.275 (67.5) | 0.034 (8.5) | 0.098 (24) | 0 |
| C/W(110)[112] | 0.176 (58) | 0.060 (20) | 0.068 (22) | 0 |
| W(111)[189] | 0.350 (85) | 0.048 (12) | 0.013 (3) | 0 |
| C/W(111)[189] | 0.155 (55) | 0.087 (31) | 0.038 (14) | 0 |
| Pt/C/W(111) | 0.091 (51) | 0.086 (49) | 0 (0) | 0 |
| C/Ti(0001)[185] | detected | 0 | detected | detected |
| C/V(110)[185] | detected | 0 | detected | 0 |

were similar to those obtained for water on ZrC(100), where the dissociative adsorption of water on ZrC-(100) was observed only after the formation of the ZrO-like layer.[180,181] The observed activity of TiC(111) and ZrC(111), and the inactivity of TiC(100) and ZrC-(100), contributed to a better understanding of the reactivity of groups 4 and 5 TMC surfaces toward oxygenated molecules. Combined with previous UPS results on NbC surfaces,[188] these investigations led to the conclusion that the (111) surfaces of groups 4 and 5 carbides were generally more active toward the dissociation of oxygenated molecules than the (100) plane. This conclusion was further supported by theoretical studies using the extended Hückel tight binding calculation to compare the active TiC(111) surface with the relatively inactive TiC(100) surface.[20]

The reaction mechanisms of methanol on C/Mo-(110),[182] C/W(110),[110,112] and C/W(111)[110,189] have been investigated extensively due to the potential of utilizing Mo and W carbides as electrocatalysts in DMFCs. All three surfaces were found to be very active toward the dissociation of methanol, as indicated by the formation of the methoxy species at liquid nitrogen temperature. Combined TPD, AES, and HREELS studies revealed three potential decomposition pathways for methoxy: (1) complete decomposition to produce atomic C and O, and gas-phase hydrogen; (2) the scission of the C−H bonds to produce CO and gas-phase hydrogen; and (3) the cleavage of the C−O bond to produce atomic O and methane. The product selectivity of methanol is summarized in Table 6 for several clean and carbide-modified Mo(110), W(110), and W(111) surfaces. In brief, these values were derived by correlating the $H_2$ desorption peak from TPD experiments to the C and O signals from AES measurements. Detailed quantitative analysis of methanol decomposition on these surfaces can be found in the respective references. Table 6 also listed the reaction pathways of methanol on C/Ti(0001) and C/V(110), although the selectivity on these two surfaces could not be quantified due to the inward diffusion of C, O, and H.[185] The comparison in Table 6 clearly indicates that the selectivity toward different reaction pathways of methanol varies noticeably on different carbide surfaces. Detailed descriptions for deriving the activity and selectivity values can be found in the respective references.

As shown in Table 6, the dominant reaction pathway of methanol on clean W(111) was the complete decomposition to produce atomic C and O, and gas-phase hydrogen.[110,189] The thermal behavior of $CH_3OH$ on C/W(111) was generally similar to that of the clean W(111) surface. The presence of carbide reduced the overall decomposition activity from 0.411 to 0.280 $CH_3OH$ molecules reacting per W atom. In addition, the selectivity values toward CO and methane on C/W(111) increased to 31 and 14%, respectively. Because the carbide surfaces would most likely be partially oxidized under the fuel cell operating conditions, the effect of oxygen modification on C/W(111) was also investigated. A parallel study of the effect of oxygen modification indicated that the O/C/W(111) surface remained active toward the dissociation of methanol, although the decomposition activity was reduced to 0.236 molecules per W atom, and CO production became the dominant pathway.[189]

Comparative investigations of C/W(111) and C/W-(110) showed only relatively minor differences in the reaction pathways of methanol.[110,112,189] TPD measurements revealed that C/W(110) was similar to C/W(111) in terms of the overall decomposition activity. The different crystal planes showed slight variations in product selectivity, as compared in Table 6. For example, although both C/W(110) and C/W(111) surfaces showed ~55% selectivity toward complete decomposition, the C/W(110) surface yielded similar amounts of CO (20%) and $CH_4$ (22%), while the C/W(111) surface produced more CO (31%) than $CH_4$ (14%).

The C/Mo(110) surface showed significant differences in terms of the product selectivity.[182] As shown in Table 6, the reaction pathway leading to the formation of methane, an undesirable reaction in the electrooxidation of methanol, was inhibited on the C/Mo(110) surface. The absence of methane production on C/Mo(110) could also explain the promotion effect reported by Kudo et al., who incorporated molybdenum carbides into tungsten carbides as a promoter in DMFC studies.[9−11]

The reaction of methanol was also conducted to explore the possible synergistic effect of depositing submonolayer Pt onto the C/W(111) surface.[81] While the presence of submonolayer Pt decreased the overall decomposition activity from 0.280 to 0.177 methanol molecules per W atom, the Pt-modified C/W(111) surface no longer produced gas-phase methane. The synergistic effect is demonstrated in Figure 6, which compares the HREEL spectra following the adsorption and decomposition of methanol on C/W(111) and on Pt/C/W(111) with a Pt coverage equivalent to 0.6 ML (monolayer). On C/W(111), the HREEL spectrum

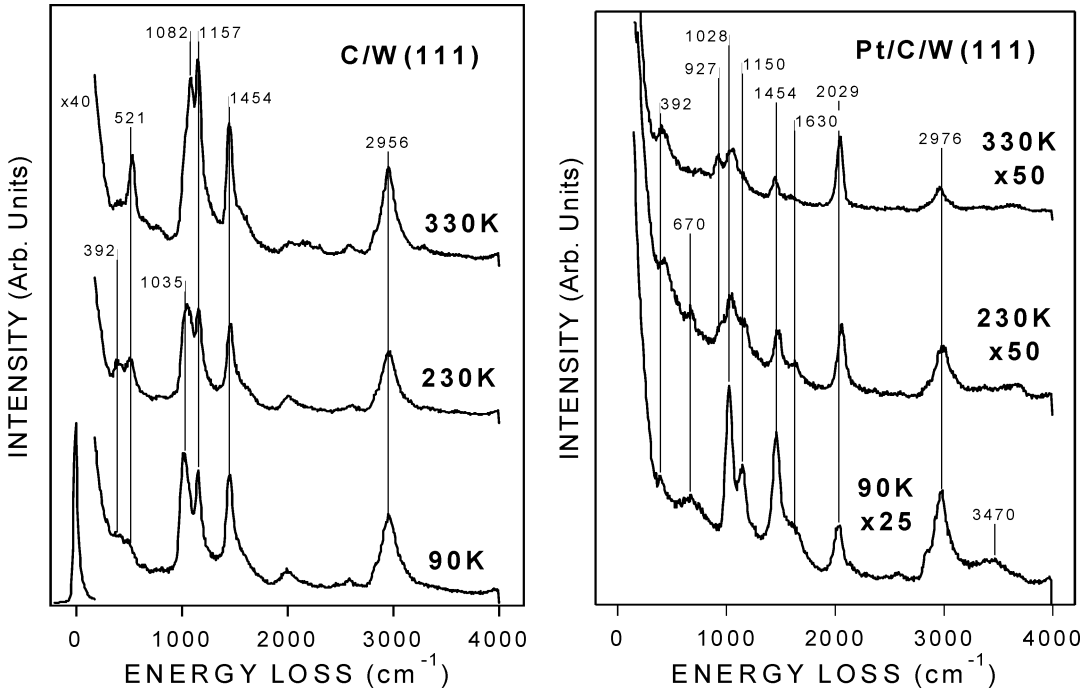


**Figure 6.** Comparison of HREEL spectra monitoring the thermal decomposition of $CH_3OH$ on (a) C/W(111)[189] and (b) Pt/C/W(111).[81] The surfaces were exposed to submonolayer coverage of methanol at 100 K followed by heating to the indicated temperatures.

at 90 K was characteristic of the methoxy ($CH_3O$) intermediate, indicating that the C/W(111) surface was very reactive toward the dissociation of the O−H moiety in methanol even at liquid nitrogen temperature. The HREEL spectra at higher temperatures indicated that the methoxy intermediate was stable up to 330 K, with the minor changes in the relative intensities being related to changes in the orientation of adsorbed methoxy.[189]

By comparing the corresponding HREEL spectra on Pt-modified C/W(111),[81] it was clear that the decomposition pathway of methanol was significantly altered when the C/W(111) surface was modified by 0.6 ML (monolayer) of Pt: (1) The 0.6 ML Pt/C/W(111) surface was somewhat less active than C/W(111) toward the scission of the O−H bond, as indicated by the presence of a relatively weak $\nu$(O−H) mode of molecular methanol on Pt/C/W(111) at 90 K. (2) On the other hand, the presence of the 0.6 ML Pt enhanced the subsequent decomposition of methoxy, as indicated by the significant decrease in the intensities of the methoxy vibrational modes on 0.6 ML Pt/C/W(111) between 230 and 330 K. In other words, the C/W(111) was more active than Pt toward the initial dissociation of the O−H bond of methanol, while Pt was more active than C/W(111) toward the subsequent dissociation of the C−H bonds in methoxy. As a result, the Pt/C/W(111) surface was more active than either Pt[190,191] or C/W(111)[189] toward the complete decomposition of methanol at temperatures below 330 K, clearly indicating a synergistic effect by supporting submonolayer coverages of Pt on C/W(111).[81]

The decomposition of methanol on a WC film, prepared by PVD synthesis on a glassy carbon substrate, was recently studied using TPD and HREELS.[17] The fundamental surface science study on PVD films demonstrated one of the first examples in bridging the "materials gap" between single crystal surfaces and polycrystalline films. Due to the fact that PVD films were not as well ordered as single crystal surfaces, HREELS measurements on PVD films were largely unexplored. By using a model LK3000 HREELS spectrometer (typical spectral resolution of 30 $cm^{-1}$ at an intensity of $10^6$ counts/second on single crystal surfaces), Zellner et al. were able to obtain relatively high quality HREELS data from the reaction of methanol on WC films, as shown in Figure 7. The HREEL spectra were characterized by excellent spectral resolution and adequate signal-to-noise. The vibrational spectra at 200 K on both WC and Pt/WC surfaces correspond to the methoxy ($CH_3O$) intermediate, indicating that both surfaces were very reactive toward the dissociation of the O−H bond in methanol. More interestingly, the presence of Pt on WC enhances the subsequent dissociation of methoxy on the Pt/WC surface between 400 and 500 K, as demonstrated by the decrease in the intensity of the methoxy vibrational modes on Pt/WC. Therefore, similar to those observed on the Pt/WC/W(111) single-crystal surface (Figure 6), the results in Figure 7 confirmed the promoting effect by depositing Pt on the WC film.[17]

The reactions of other alcohol molecules, such as ethanol and 2-propanol, were studies on TiC(100) and VC(100) using TPD and HREELS.[193] Both surfaces showed some dissociative activity toward ethanol and 2-propanol upon adsorption at 100 K, although the TiC(100) surface appeared to be slightly more active at this temperature. By 153 K, alkoxy intermediates from ethanol decomposition were detected with HREELS on both TiC(100) and VC(100). When heated to higher temperatures, the dehydration of the alkoxy intermediates produced gas-phase

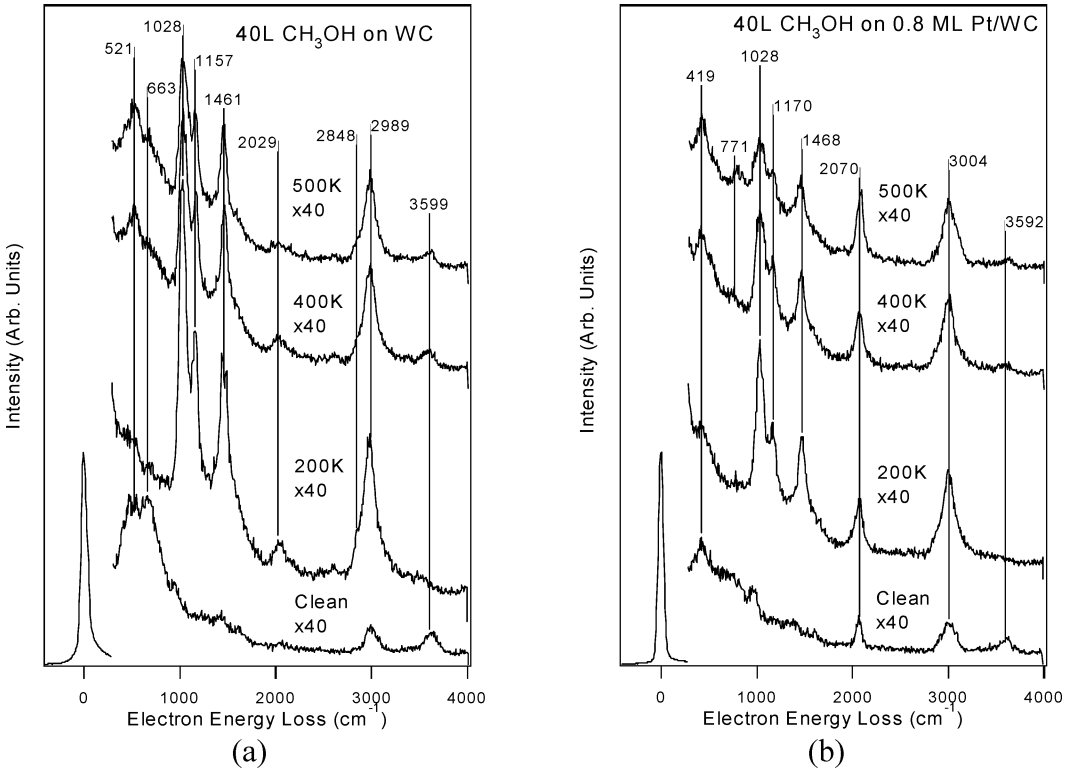


**Figure 7.** HREEL spectra monitoring the thermal decomposition of $CH_3OH$ on PVD films[17] of (a) WC and (b) 0.8 ML Pt/WC. The Pt/WC surface was prepared by evaporating Pt onto a clean PVD WC film at 600 K.

alkenes as the dominant reaction products. Although it was less active at 100 K, the VC(100) surface was estimated to be ~20% more active toward the production of alkenes than TiC(100). This observation was similar to the comparative investigation of the dissociation of methanol on the two surfaces by the same authors, as described earlier.[183] Moreover, isotopic studies revealed that $\gamma$-hydride elimination was a critical step in the formation of gas-phase alkene from adsorbed ethanol.[193] Additional AFM studies of ethanol adsorbed on VC(100) showed approximately 40% reduction in the frictional forces when compared to the case of the unmodified VC-(100) surface.[194] Related frictional response studies were also conducted on VC(100) after the adsorption of 1-octanol and 2,2,2-trifluoroethanol.[195] Perry and co-workers noted that, upon adsorption of 2,2,2-trifluoroethanol at room temperature, the surface exhibited both an increase in friction and a decrease in adhesion. The higher frictional response was attributed to the shear strength of the multilayer adsorbate film. On the other hand, the reduced adhesion could be due to the increase in surface roughness and a lowering of surface free energy.[195] These authors also utilized similar approaches to investigate the interaction of a model lubricant additive, trimethyl phosphate, on the TiC(100) and VC(100) surfaces.[196]

### 5.3. Carbon Dioxide

The interaction between $CO_2$ and $Mo_2C$/Mo(100) was investigated using HREELS, TPD, and XPS.[197] The adsorption of $CO_2$ onto $Mo_2C$/Mo(100) did not result in any changes in the surface work function. Vibrational studies exhibited features at 660 and ~2355 $cm^{-1}$, which were characteristic vibrations of unperturbed $CO_2$. Additional TPD measurements showed only a single desorption peak at 190 K. In contrast, when the $Mo_2C$/Mo(100) surface was covered by potassium, Solymosi and co-workers observed a decrease in the work function by as much as 3.3 eV. Furthermore, HREELS results showed losses at ~750, ~1220, and ~1600 $cm^{-1}$, which were ascribed to the formation of the $CO_2^-$ radical.[197] These results generally agreed with previous investigations of the adsorption of $CO_2$ on K-covered Pt-group metal surfaces.[198−200]

## 6. Reactions with Sulfur-Containing Molecules

The removal of sulfur from the hydrocarbon feeds via hydrodesulfurization (HDS) is critical in preserving the catalyst activities in refinery processes.[204] Typically sulfur is found in the form of thiols, sulfides, and thiophenes,[205] which are usually abated with a mixture of cobalt and molybdenum sulfide catalysts supported on $\gamma$-alumina.[204,206,207] Recent reactor studies have demonstrated that supported molybdenum carbides possess HDS activity over twice that of a commercial Ni-promoted $MoS_x$ catalyst.[208] Reactivity studies of model catalyst surfaces using simple probe molecules have provided valuable insights into industrial processes. For example, thiophene[209−211] and $SO_2$[212,213] are molecules often used to model HDS and De-$SO_x$ processes, respectively.

### 6.1. Thiophene

The chemistry of thiophene ($C_4H_4S$) has been studied over a C/Mo(110) surface by Rodriguez et al.

using synchrotron-based soft-XPS.[211] Exposures of thiophene at 100 K produced S 2p features characteristic of physisorbed and chemisorbed thiophene between 166.5 and 164.5 eV; the decomposition of thiophene had not taken place at this temperature, as evidenced by the absence of atomic S features at 163.5 and 161.5 eV. Heating to 170 K resulted in the desorption of physisorbed $C_4H_4S$. The decomposition of thiophene occurred between 200 and 250 K, producing atomic S and $C_xH_y$ fragments on the surface. The $C_xH_y$ fragments further decomposed at higher temperatures, with the carbon eventually migrated into the bulk. The strongly bonded atomic sulfur could only be removed after heating the surface to above 2200 K.[211] Overall, the reactivity of the C/Mo(110) surface toward $C_4H_4S$ was similar to that of clean Mo(110).[214]

The decomposition of thiophene on an α-$Mo_2C$-(0001) single-crystal surface was investigated by St. Clair et al. using TPD measurements.[210] The desorption of the hydrogen product was detected at 435 and 600 K, with the first peak being desorption-limited and the second being reaction-limited. These authors attributed the first $H_2$ signal to the decomposition of thiophene and the second to the subsequent dehydrogenation of surface $C_xH_y$ fragments. The decomposition of thiophene was confirmed by additional XPS and UPS studies, which indicated that the scission of C−S bonds occurred at a temperature of 170 K or lower.[210]

## 6.2. Alkanethiol

The reactions of $H_2S$ and $CH_3SH$ on C/Mo(110) have been investigated to further understand the interaction between sulfur-containing molecules and carbide surfaces..[212] Using SXPS, Rodriguez and co-workers showed that C/Mo(110) is active toward the S−H and S−C bond scission at temperatures below 300 K. Upon $H_2S$ adsorption at 100 K, the S 2p spectrum indicated the presence of a physisorbed state and two chemisorbed species. Between 150 and 200 K, a significant portion of the chemisorbed $H_2S$ dissociated to atomic S and HS, and only atomic sulfur was present on the C/Mo(110) surface by 350 K. For comparison, the scission of the S−H bond in the adsorbed $CH_3SH$ species most likely took place immediately upon adsorption at 100 K. Between 100 and 350 K, $CH_3S$ and $CH_yS$ intermediates coexisted on the carbide surface. Heating to 500 K resulted in further decomposition, which led to the desorption of methane, the incorporation of some carbon into the bulk, and the deposition of atomic S on the surface. Overall, the reactivities of the C/Mo(110) surface toward $H_2S$ and $CH_3SH$ were generally similar to those reported on clean Mo(110).[215] Rodriguez et al. suggested that the strong activity of the carbide surface toward sulfur-containing molecules can be attributed to the fact that metal centers in C/Mo(110) are in a low oxidation state and have a large density of 4d states near the Fermi level.[212]

The reactions of alkanethiols, specifically ethanethiol[216] and 1,2-ethanedithiol,[217,218] on C/Mo(110) have been studied by Roe and Schulz. While ethanethiols are not a prominent component in crude oil feeds, they were chosen as probe molecules to provide insights into the chemistry of sulfhydryl (SH) groups on carbide surfaces. Prior studies of ethanethiol on clean Mo(110) showed the formation of an ethanethiolate intermediate at 120 K.[219] The ethanethiolate intermediate on clean Mo(110) subsequently decomposes to yield gas-phase ethane and ethylene. A fraction of the surface intermediate also underwent complete decomposition to produce surface carbon and sulfur, and gas-phase hydrogen.[216] Roe and Schulz also examined the effect of defects on the commonly studied (4 × 4)-C/Mo(110) surface. The authors characterized the surface as "defective", as the LEED pattern showed certain missing spots from an ideal (4 × 4) overlayer. TPD measurements following low-temperature adsorption of ethanethiol on the "defective" (4 × 4)-C/Mo(110) surface revealed no major differences in terms of activity and selectivity when compared to those obtained on clean Mo-(110). A broad ethylene desorption peak was observed between 200 and 400 K while ethane desorption was detected at 375 K. Roe and Schulz then examined the effect of sulfur coverage on the ethanethiol chemistry. As expected, the presence of surface sulfur reduced the amount of ethylene and ethane produced; the desorption temperatures of ethylene and ethane also shifted to higher temperatures with increasing sulfur coverage.[216]

The reaction of 1,2-ethanedithiol on the C/Mo(110) surface produced gas-phase ethylene and acetylene, and atomic sulfur.[217,218] Unlike the chemistry of ethanethiol described above, significant differences were observed in the reaction pathways between clean Mo(110) and C/Mo(110) surfaces. In addition to the ethylene and acetylene products that were produced on clean Mo(110), the dissociation of 1,2-ethanedithiol on C/Mo(110) also led to the formation of gas-phase vinyl thiol and ethanethiol products. The authors suggested that while clean Mo(110) dissociated only a fraction of the C−S bonds, the C/Mo(110) surface facilitated the complete desulfurization of ethanedithiol, leading to the desorption of non-sulfur-containing hydrocarbons.[217]

## 6.3. $SO_2$

The dissociation pathway of $SO_2$ on C/Mo(110) was investigated by Rodriguez and co-workers using SXPS.[212] At 150 K the XPS S 2p spectrum showed the presence of atomic sulfur, $SO_2$, and a mixture of $SO_3$ and $SO_4$. Between 200 and 500 K, the features attributed to $SO_x$ species decreased as the intensity for atomic sulfur increased. The atomic S and O resulting from the dissociation of $SO_x$ remained on the surface even after heating to 1200 K. Corresponding NEXAFS measurements following $SO_2$ decomposition on $Mo_2C$ powders also showed similar reaction mechanisms to those on C/Mo(110).[212]

Rodriguez and co-workers also extended their $SO_2$ studies to the TiC(001) surface.[220] Photoemission and TPD measurements revealed that most of the $SO_2$ desorbed molecularly below room temperature, although a fraction (<35%) of the adsorbates underwent dissociation to produce surface S and O atoms at temperatures near 400 K. Parallel DFT calcula-

tions suggested that C−S and C−O interactions are essential for the dissociation of $SO_2$ on the TiC(001) surface.[220,221] A related theoretical study also compared the reactivity of $SO_2$ on three titanium carbides, metcar $Ti_8C_{12}$, nanocrystal $Ti_{14}C_{13}$, and bulk TiC(001).[221] Using DFT-GGA calculations, the authors showed that $Ti_8C_{12}$ was the most reactive toward $SO_2$ dissociation, followed by $Ti_{14}C_{13}$ and then the TiC(001) surface. Compared with other studies on metal oxides,[222,223] the various titanium carbide substrates were more efficient toward the dissociation of $SO_2$. The results also clearly indicated that the carbon atoms in carbides directly influenced the desulfurization process by stabilizing the S and O adatoms.[221]

## 7. Reactions with Nitrogen-Containing Molecules

### 7.1. Ammonia

The interaction of ammonia with TiC(100) and VC(100) surfaces has been studied by Fernandez-Torres et al. using TPD, HREELS, and UPS.[224] On TiC(100), $NH_3$ desorbed at 230 K at low coverages and at 211 K at near saturation coverage. The authors observed no evidence for the decomposition of $NH_3$ up to 773 K, as the TPD measurements monitoring the $H_2$ and $N_2$ products showed no desorption features within this temperature range. At 153 K, the HREEL spectra of $NH_3$ adsorbed on TiC(100) exhibited energy loss features at 1075, 1570, 3300, and 3400 $cm^{-1}$, which were attributed to the symmetric $NH_3$ bending, the asymmetric $NH_3$ bending, $\nu_s$(N−H), and $\nu_{as}$(N−H) modes, respectively. The observation of an intense $NH_3$ bending mode suggested that $NH_3$ adsorbed with the $C_3$ axis perpendicular to the surface. The authors also noted that ammonia most likely bonded to the metal sites on TiC(100), as indicated by the absence of surface C−N vibrational modes and by the fact that the metal sites would accept electrons more readily than the carbon sites. Additional UPS experiments revealed two features at 6.4 and 10.6 eV, which corresponded to the $3a_1$ and 1e orbital emissions, respectively, of molecularly adsorbed $NH_3$.

The adsorption of $NH_3$ on VC(100) yielded essentially the same results as those on TiC(100).[224] At saturation coverage, two monolayer desorption features were detected from VC(100) at 211 and 273 K, with the latter being attributed to $NH_3$ adsorbed on defect sites. As was the case on TiC(100), no N−H bond activation was observed on VC(100). These results were consistent with the modeling of electronic structures of the TiC(100) and VC(100) substrates, which suggested similar vacant electronic orbitals available to interact with the lone pair of $NH_3$.[34,224]

### 7.2. Nitrile

The reactions of HCN[225,226] and acetonitrile ($CH_3CN$)[227,228] provided insights into the activation of the nitrile functional group on carbides. Friend and coworkers used XPS, TPD, and HREELS to examine the surface reactions of HCN on clean and carbide-modified W(100).[225,226] A variety of competing reaction pathways exist between 200 and 500 K: (1) molecular desorption of HCN, (2) formation of adsorbed HCNH, and (3) complete decomposition of HCN yielding gas-phase hydrogen, and surface carbon and nitrogen. Heating to temperatures above 600 K resulted in recombinatory desorption of HCN. By 1500 K, the original carbide surface was retained as atomic nitrogen recombined and desorbed as $N_2$ from the surface.[225,226]

Parallel studies of acetonitrile showed that, aside from molecular desorption, a $CH_2CNH$ surface intermediate was formed following the selective formation of an N−H bond and cleavage of a C−H bond at ~400 K.[227,228] This surface species subsequently underwent three competing reaction pathways: (1) complete decomposition to atomic nitrogen, carbon, and gas-phase hydrogen; (2) isomerization back to acetonitrile, followed by desorption; and (3) scission of either N−H or C−H bonds to form HNC or HCN, carbon, and gas-phase hydrogen. Compared to the clean W(100) surface, the carbide surface was less selective toward the complete decomposition pathway. As a result, significant amounts of molecularly intact fragments were produced from the C/W(100) surface.[227,228]

## 8. Correlating Surface Reactivity with Electronic Properties

### 8.1. Similarities and Differences between TMC and Pt-Group Metal Surfaces

From the chemical reactivities summarized in sections 3−7, it is clear that the presence and/or incorporation of carbon atoms can significantly modify the chemical properties of groups 4−6 early transition metals. In most cases, the formation of carbides appears to "tame" the high chemical activity of the early transition metal surfaces. This is especially obvious in studies using hydrocarbon molecules as probe reactions (section 4). For example, groups 4−6 early transition metals bond strongly to ethylene in the di-$\sigma$ configuration, which undergoes subsequent dissociation to atomic carbon and hydrogen without the cleavage of the metal−carbon bonds. In contrast, the formation of the ethylidyne ($CCH_3$) intermediate on TMC surfaces indicates the rupture of one of the metal−carbon bonds in di-$\sigma$ bonded ethylene, suggesting that the ethylene/surface complex is less strongly bonded on TMC than that on the corresponding clean metals. Another example is the reaction of cyclohexene. On groups 4−6 metals, di-$\sigma$ bonded cyclohexene molecules undergo complete dissociation to atomic carbon and hydrogen without producing any gas-phase hydrocarbon products. In contrast, a significant fraction of di-$\sigma$ bonded cyclohexene dehydrogenates to produce gas-phase benzene, again indicating weaker metal−adsorbate bonds on the TMC surfaces. Therefore, the formation of carbides on groups 4−6 metals reduces the degree of interaction between adsorbates and TMC surfaces, leading to a modified surface activity that more closely resembles the Pt-group metals than the parent metals.

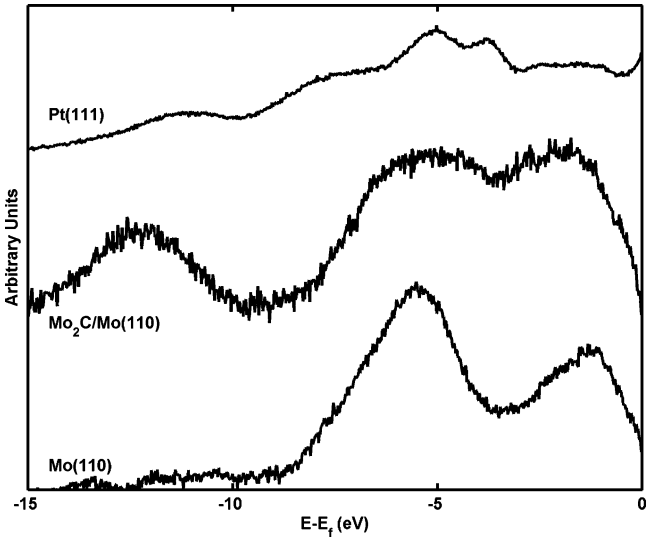


**Figure 8.** SXPS comparing the density of states (DOS) near the Fermi level of Mo(110), C/Mo(110), and Pt(111).[61] The incident photon energy was 150 eV for the Mo valence states.

The description of "Pt-like" properties of TMC surfaces is, however, clearly an oversimplification. For example, in the case of the formation of ethylidyne from ethylene, the thermal stability and adsorption geometry of ethylidyne on TMC surfaces are noticeably different from those on Pt(111). In addition, in the case of the selective dehydrogenation of cyclohexene to produce benzene, the desorption temperature and the desorption mechanism (reaction-limited vs desorption-limited) on TMCs are different from those on the Pt-group metal surfaces. Furthermore, in reactions involving oxygen-containing molecules (section 5), the TMC surfaces are significantly more active than the Pt-group metal surfaces.

The electronic properties of TMC and Pt-group metal surfaces, especially the density of states (DOS) near the Fermi level, also appear to be different. For example, Figure 8 shows the SXPS spectra of Mo(110), C/Mo(110), and Pt(111).[61] The comparison between Mo(110) and C/Mo(110) reveals a significant modification of the DOS of Mo(110) upon the formation of carbide. For the C/Mo(110) surface, the valence state is characterized by two overlapping peaks at ~5.7 and ~1.9 eV, which are related to emissions from the hybridized Mo and C states as assigned in previous studies.[43,229,230] A new feature is also present on C/Mo(110) at approximately 12.5 eV below the Fermi level, which is due to contributions from the C 2s states.[61] More importantly, the comparison between the SXPS spectra of C/Mo(110) and Pt(111) clearly shows differences between the two surfaces in terms of peak positions and relative intensities of features near the Fermi level. The interpretation of the SXPS results requires the assistance of theoretical modeling, as described below.

## 8.2. Theoretical Modeling of Surface Properties

As mentioned in sections 2−7 and summarized in Tables 1 and 2, theoretical investigations, in particular DFT modeling, have been the subject of many investigations to correlate the electronic and chemical properties of TMC surfaces. For example, the theoretical investigations have revealed different electronic properties between TiC(100) and TiC(111)[20,22,34] and between TiC(100) and VC(100),[34] which have in turn been utilized to successfully explain the different chemical activities between these surfaces.

DFT modeling has also played an important role in understanding the effect of carbon/metal stoichiometry on the electronic, structural, and chemical properties in TMCs. For example, Didziulis et al. have recently compared the electronic properties of $Ti_8C_8$, $Ti_9C_9$, $Ti_{13}C_{13}$, and $V_9C_9$ clusters to further highlight the different electronic properties between Ti and V carbides.[34] Rodriguez and co-workers have provided significant insights by systematically comparing the properties of "metcar" $Ti_8C_{12}$, nanocrystal $Ti_{14}C_{13}$, and bulk TiC(001).[39,221,231] These authors have recently performed additional DFT modeling on the electronic and chemical properties of another "metcar" compound, $Mo_8C_{12}$, to determine the effect of carbon in group 6 metal carbides.[40,232,233] The utilization of the "metcar" nanostructures as model systems will continue to be an area of interest in the DFT modeling of TMC.[234−237]

Several recent studies have attempted to correlate the center of the metal d-band to the chemical activities of TMC surfaces.[61,238,239] For example, Rodriguez and co-workers have recently correlated the shift in the d-band center from Mo(001) to $\gamma$-MoC(001) with the adsorption energy of CO and atomic sulfur.[238] These studies have been inspired by the work of Nørskov and co-workers, who have demonstrated a strong correlation between the center of the d-band and the surface reactivity of transition metals and alloys.[240,241] More recently, such a correlation has been extended to bimetallic surfaces with the monolayer film of the second metal residing either on the surface or in the subsurface region.[242,243]

One of the advantages of utilizing the d-band center as a parameter for the electronic properties of TMCs is that it can be measured experimentally, such as using SXPS. The direct comparison of the DFT modeling results with experimental measurements provides a critical validation of the modeling work. For example, Figure 9 compares the occupied states derived from DFT modeling with the SXPS measurement for C/Mo(110).[239] The DFT result is obtained using a C-terminated $Mo_2C(0001)$ surface as shown earlier in Figure 1d. Because the estimation of the d-band center involves the overall average of both the occupied and unoccupied states, SXPS alone cannot provide a direct comparison with the theoretically predicted d-band center. Techniques such as ARPES or inverse photoemission spectroscopy will be needed to determine the density of the unoccupied states. Nevertheless, the comparison between DFT modeling and SXPS measurements, as shown in Figure 9, provides a validity test of the occupied states between theoretical and experimental results.

Another obvious advantage of using the d-band center model is that it allows a direct comparison of the electronic and chemical properties of TMC surfaces with those of Pt-group metals and alloys. For

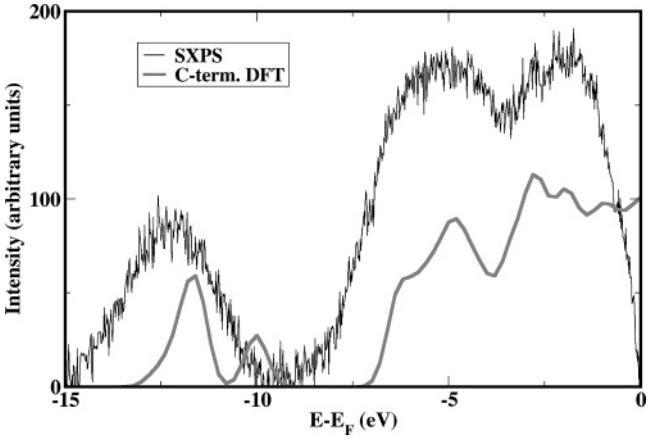


**Figure 9.** Comparing the SXPS spectrum of C/Mo(110) with the DFT calculated spectrum of carbon-terminated $Mo_2C(0001)$.[239] Details of the DFT modeling are described in the text.

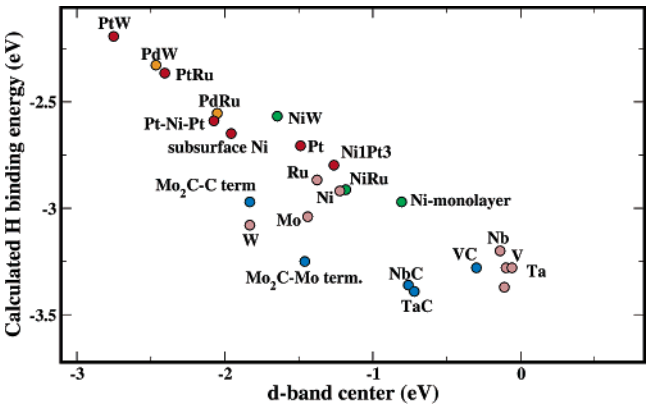


**Figure 10.** Correlation of HBE with the d-band centers of TMC and bimetallic surfaces.[61,239,242,243] The d-band centers were determined using a short cutoff radius of 1 Å for all surfaces.

example, Figure 10 shows the correlation between the calculated hydrogen binding energy (HBE) and the d-band center for several bimetallic alloys and metal carbides. For comparison, the values for the corresponding monometallic components are also included. Figure 10 shows that the HBE decreases nearly linearly as the d-band center shifts away from the Fermi level on monometallic and bimetallic transition metal surfaces.[240−243] The general trend in the DFT results in Figure 10 has been verified experimentally on several bimetallic surfaces by TPD studies of the desorption of hydrogen.[244−246] Furthermore, it is well established that the general trend shown in Figure 10 can be extended to the adsorption strength of many other inorganic and organic molecules on monometallic and bimetallic surfaces.[240,241] Therefore, establishing a correlation between the HBE and the d-band center of TMC surfaces would significantly enhance the understanding and predictability of the chemical properties of TMC surfaces. The values for the groups 4 and 5 TMC surfaces in Figure 10 are calculated using the metal-terminated fcc(111) surfaces; the values for the group 6 $Mo_2C$ are obtained using both C- and Mo-terminated surfaces.[61,239] The general trend in Figure 10 is that the d-band center of a TMC shifts away from the Fermi level as compared to the case of the corresponding parent metal surface, which is consistent with the experimental observation that the TMC surface is less active than the parent metal. Calculations on other TMC surfaces, such as the fcc(100) and C-terminated fcc(111) surfaces, are necessary to establish whether a near linear correlation exists for the TMC surfaces.

While the results in Figure 10 suggest that the d-band center shifts away from the Fermi level as compared to the case of the corresponding parent metals, it is important to point out this shift in carbides is more complicated than that in bimetallic surfaces. This is because the formation of the metal−carbon bonds often leads to a charge transfer from metal to carbon. The resulting decrease in the d-band filling would most likely shift the d-band center toward, instead of away from, the Fermi level. Rodriguez and co-workers have suggested the possible origin for the shift of the d-band center in carbides.[238] They pointed out that the strong interaction with carbon should broaden the d-bandwidth of the parent metal and therefore shift the d-band center away from the Fermi level. More systematic DFT modeling is clearly necessary to achieve a general correlation of the d-band centers in various carbide surfaces.

Although the d-band center model offers the potential to correlate the electronic and chemical properties of TMC surfaces, it is important to point out that little is understood in this area at present. The presence of carbon in TMC can induce both electronic and structural modifications, at least in the following three effects: (1) The electronic interaction between the valence states of carbon and the parent metal modifies the density of states near the Fermi level. (2) The incorporation of carbon typically increases the metal−metal distance as compared to that of the parent metal, which causes a tensile strain in the metal lattice and should lead to additional modification of the metal d-band.[247] (3) The presence of carbon atoms in or on the surface reduces the number of surface metal sites available for the adsorption and subsequent reactions of molecules. All three effects should lead to modifications of the surface reactivity of TMCs compared to their parent metal surfaces. Additional theoretical and experimental studies are needed to decouple these different effects.

## 9. Future Research Opportunities

As summarized in the current review, surface science studies have significantly enhanced the fundamental understanding of the intriguing chemical properties of TMC surfaces. The combined experimental and theoretical investigations have led to some correlations, although mostly qualitative at present, between the electronic properties and surface reactivities. The authors firmly believe that TMC surfaces will provide fruitful and challenging opportunities for future surface science studies, in particular in the following three areas:

(1) As model systems to determine quantitative correlations between the electronic and chemical properties. As pointed out in the previous section, the

formation of carbides on groups 4−6 metals can modify the electronic and structural properties of the parent metals, both of which can lead to modified chemical activities. More concerted experimental studies and theoretical modeling are needed to decouple these effects. Furthermore, these studies should also lead to a deeper understanding of the roles of the metal d-band, such as the d-band center, in controlling the adsorption/reaction of molecules on TMC surfaces. The results from these studies should enhance our understanding of the fundamental correlation between electronic and chemical properties not only for TMC surfaces but also for transition metals in general.

(2) As examples to bridge the "materials gap" between single-crystal surfaces and "real world" catalytic materials. Previous studies have demonstrated that stoichiometric PVD films[17] and metcar nanoclusters[236] can be synthesized relatively easily and can be utilized as model systems for polycrystalline TMC surfaces and supported TMC particles, respectively. The structural, electronic, and chemical properties of the PVD films and metcar clusters can be readily investigated using a battery of experimental and theoretical surface science techniques. The fundamental understanding from these studies should provide a critical link between single-crystal surfaces and TMC catalysts.

(3) As model surfaces to determine the feasibility of TMCs as potential catalysts and electrocatalysts. In addition to the "Pt-like" properties, TMC materials are attractive catalysts because of their tolerance to sulfur poisoning[248,249] and resistance to coke formation.[250,251] Recent studies using TMCs as catalysts for steam reforming[249,250] and as electrocatalysts for fuel cells[17] have further renewed these interests. Surface science studies of carefully chosen probe molecules will identify whether TMC surfaces possess desirable reaction pathways over those on unmodified transition metals. In addition, surface science investigations of the chemical stability of TMCs, especially under in-situ conditions, will provide important insights into the feasibility and experimental conditions for using TMCs as catalysts and electrocatalysts. Finally, further studies of the synergistic effect by depositing submonolayer Pt-group metals on TMC surfaces[81,162] will identify the possibility of using TMCs as catalyst supports for catalytic and electrocatalytic applications.

## 10. Acknowledgment

We acknowledge financial support from Basic Energy Sciences of the Department of Energy (DOE/BES Grant No. DE-FG02-04ER15501). H.H.H. acknowledges financial support from the Presidential Fellowship at the University of Delaware. We would also like to acknowledge those authors who provided preprints prior to publication. We thank John Kitchin for discussion of the DFT modeling of carbide surfaces. Finally, J.G.C. would like to thank his former and current graduate students and postdoctoral fellows for their contributions.

## 11. Appendix: List of Abbreviations of Characterization Techniques

| | |
|---|---|
| AES | Auger electron spectroscopy |
| AFM | atomic force microscopy |
| ARPES | angle-resolved photoemission spectroscopy |
| ARUPS | angle-resolved ultraviolet photoelectron spectroscopy |
| ARXPS | angle-resolved X-ray photoelectron spectroscopy |
| CLPES | core-level photoemission spectroscopy |
| DFT | density functional theory |
| HREELS | high-resolution electron energy loss spectroscopy |
| ISS | ion scattering spectroscopy |
| ICISS | impact-collision ion scattering spectroscopy |
| IRAS (RAIRS) | infrared reflection absorption spectroscopy |
| IR−REMPD | infrared resonance-enhanced multiphoton dissociation |
| IR−REMPI | infrared resonance-enhanced multiphoton ionization |
| LEED | low-energy electron diffraction |
| MS | mass spectrometry |
| NEXAFS (XANES) | near-edge X-ray absorption fine structure |
| RHEED | reflection high-energy electron diffraction |
| STM | scanning tunneling microscopy |
| SXPS | soft X-ray photoelectron spectroscopy |
| THEED | transmission high-energy electron diffraction |
| TPD | temperature-programmed desorption |
| TOF-MS | time-of-flight mass spectrometry |
| UPS | ultraviolet photoelectron spectroscopy |
| XAS | X-ray absorption spectroscopy |
| XPS | X-ray photoelectron spectroscopy |
| XRD | X-ray diffraction |

## 12. References

(1) Toth, L. E. *Transition Metal Carbides and Nitrides*; Academic Press: New York, 1971.
(2) Oyama, S. T. *Catal. Today* **1992**, *15*, 179.
(3) Gubanov, V. A.; Ivanovsky, A. L.; Zhukov, V. P. *Electronic Structure of Refractory Carbides and Nitrides*; Cambridge University Press: Cambridge, 1994.
(4) Santhanam, A. T. In *The Chemistry of Transition Metal Carbides and Nitrides*; Oyama, S. T., Ed.; Blackie Academic and Professional: Glasgow, 1996; p 28.
(5) Oyama, S. T. *The Chemistry of Transition Metal Carbides and Nitrides*; Blackie Academic and Professional: Glasgow, 1996.
(6) Chen, J. G. *Chem. Rev.* **1996**, *96*, 1497.
(7) Levy, R. L.; Boudart, M. *Science* **1973**, *181*, 547.
(8) Ross, P. N., Jr.; MacDonald, J.; Stonehart, P. *J. Electroanal. Chem.* **1975**, *63*, 450.
(9) Kudo, T.; Kawamura, G.; Okamoto, H. *J. Electrochem. Soc.* **1983**, *130*, 1491.
(10) Kudo, T.; Ishikawa, A.; Kawamura, G.; Okamoto, H. *J. Electrochem. Soc.* **1985**, *132*, 1814.
(11) Okamoto, H.; Kawamura, G.; Ishikawa, A.; Kudo, T. *J. Electrochem. Soc.* **1987**, *134*, 1645.
(12) Johansson, L. I. *Surf. Sci. Rep.* **1995**, *21*, 177.
(13) Chen, J. G. *Surf. Sci. Rep.* **1997**, *30*, 1.
(14) Tulhoff, H.; Berlin, H. C. S.; Goslar, W. *Ullmann's Encyclopedia of Industry Chemistry*; Wiley-VCH Verlag GmbH & Co.: 2000.
(15) Christensen, A. N. *Acta Chem. Scand.* **1977**, *31*, 509.
(16) Wang, J.; Castonguay, M.; Deng, J.; McBreen, P. H. *Surf. Sci.* **1997**, *374*, 197.
(17) Zellner, M. B.; Chen, J. G. *Catal. Today*, in press. Zellner, M. B.; Chen, J. G. *Surf. Sci.* **2004**, *569*, 89.
(18) Tagawa, M.; Kawasaki, T.; Oshima, C.; Otani, S.; Edamoto, K.; Nagashima, A. *Surf. Sci.* **2002**, *517*, 59.
(19) Tagawa, M.; Okuzawa, M.; Kawasaki, T.; Oshima, C.; Otani, S.; Nagashima, A. *Phys. Rev. B* **2001**, *63*, Art. No. 073407.
(20) Jansen, S. A.; Hoffmann, R. *Surf. Sci.* **1988**, *197*, 474.
(21) Edamoto, K.; Anazawa, T.; Mochida, A.; Itakura, T.; Miyazaki, E.; Kato, H.; Otani, S. *Phys. Rev. B* **1992**, *46*, 4192.
(22) Tan, K. E.; Finnis, M. W.; Horsfield, A. P.; Sutton, A. P. *Surf. Sci.* **1996**, *348*, 49.

(23) Noda, T.; Yamazaki, M.; Ozawa, K.; Edamoto, K.; Otani, S. *Surf. Sci.* **2000**, *450*, 27.
(24) Edamoto, K.; Yamazaki, M.; Noda, T.; Ozawa, K.; Otani, S. *Surf. Sci.* **2002**, *498*, 343.
(25) Ozawa, K.; Noda, T.; Nakane, T.; Yamazaki, M.; Edamoto, K.; Tanaka, S.; Otani, S. *Surf. Sci.* **2000**, *446*, 229.
(26) Edamoto, K.; Anazawa, T.; Tokumitsu, S.; Tanabe, A.; Sekine, R.; Miyazaki, E.; Kato, H.; Otani, S. *Solid State Commun.* **1996**, *97*, 435.
(27) Kitaoka, H.; Ozawa, K.; Edamoto, K.; Otani, S. *Surf. Sci.* **2002**, *511*, 359.
(28) Ozawa, K.; Ishikawa, S.; Miyazaki, E.; Edamoto, K.; Kato, H.; Otani, S. *Surf. Sci.* **1997**, *375*, 250.
(29) Ozawa, K.; Ishikawa, S.; Edamoto, K.; Kato, S.; Otani, S. *Surf. Sci.* **1999**, *419*, 226.
(30) Ozawa, K.; Anazawa, T.; Tokumitsu, S.; Sekine, R.; Miyazaki, E.; Edamoto, K.; Tanaka, S.; Otani, S. *Surf. Sci.* **1995**, *336*, 93.
(31) Larsson, C. G.; Pendry, J. B.; Johannson, L. I. *Surf. Sci.* **1985**, *162*, 19.
(32) Ozawa, K.; Yoshii, T.; Noda, T.; Edamoto, K.; Tanaka, S. *Surf. Sci.* **2002**, *511*, 421.
(33) Ozawa, K.; Ishikawa, S.; Tokumitsu, S.; Sekine, R.; Miyazaki, E.; Edamoto, K.; Kato, H.; Otani, S. *Surf. Sci.* **1996**, *364*, L612.
(34) Didziulis, S. V.; Butcher, K. D.; Perry, S. S. *Inorg. Chem.* **2003**, *42*, 7766.
(35) Lee, S.; El-bjeirami, O.; Perry, S. S.; Didziulis, S. V.; Frantz, P.; Radhakrishnan, G. *J. Vac. Sci. Technol., B* **2000**, *18*, 69.
(36) van Heijnsbergen, D.; von Helden, G.; Duncan, M. A.; van Roij, A.; Meijer, G. *Phys. Rev. Lett.* **1999**, *83*, 4983.
(37) von Helden, G.; van Heijnsbergen, D.; Duncan, M. A.; Meijer, G. *Chem. Phys. Lett.* **2001**, *333*, 350.
(38) van Heijnsbergen, D.; Duncan, M. A.; Meijer, G.; von Helden, G. *Chem. Phys. Lett.* **2001**, *349*, 220.
(39) Liu, P.; Rodriguez, J. A.; Hou, H.; Muckerman, J. T. *J. Chem. Phys.* **2003**, *118*, 7737.
(40) Hou, H.; Muckerman, J. T.; Liu, P.; Rodriguez, J. A. *J. Phys. Chem. A* **2003**, *107*, 9344.
(41) Muñoz, J.; Rohmer, M.; Bénard, M.-M.; Bo, C.; Poblet, J.-M. *J. Phys. Chem. A* **1999**, *103*, 4762.
(42) Zhang, Y. F.; Li, J. Q. *J. Chin. Chem. Soc. (Taipei)* **2003**, *50*, 517.
(43) Reinke, P.; Oelhafen, P. *Surf. Sci.* **2000**, *468*, 203.
(44) Luthin, J.; Linsmeier, Ch. *Surf. Sci.* **2000**, *454*−*456*, 78.
(45) St. Clair, T. P.; Oyama, S. T.; Cox, D. F.; Otani, S.; Ishizawa, Y. *Surf. Sci.* **1999**, *426*, 187.
(46) Göthelid, M.; Janin, E. *J. Phys.: Condens. Matter* **1999**, *11*, 773.
(47) Lo, R.-L.; Fukui, K.; Otani, S.; Iwasawa, Y. *Surf. Sci.* **1999**, *440*, L857.
(48) Sugihara, M.; Ozawa, K.; Edamoto, K.; Otani, S. *Solid State Commun.* **2002**, *121*, 1.
(49) Siegel, D. J.; Hector, L. G., Jr.; Adams, J. B. *Surf. Sci.* **2002**, *498*, 321.
(50) Smedh, M.; Diaz, S. F.; Campbell, C. T. *Phys. Rev. B* **2003**, *67*, Art. No. 205401.
(51) Young, M. B.; Slavin, A. J. *Surf. Sci.* **1991**, *245*, 56.
(52) He, J.-W.; Kuhn, W. K.; Goodman, D. W. *Surf. Sci.* **1992**, *262*, 351.
(53) Frühberger, B.; Chen, J. G.; Eng, J., Jr.; Bent, B. E. *J. Vac. Sci. Technol., A* **1996**, *14*, 1475.
(54) Frühberger, B.; Chen, J. G. *Surf. Sci.* **1995**, *342*, 38.
(55) Hwu, H. H.; Zellner, M. B.; Chen, J. G. *J. Catal.* **2005**, *229*, 35.
(56) Kapoor, R.; Oyama, S. T.; Frühberger, B.; DeVries, B. D.; Chen, J. G. *Catal. Lett.* **1995**, *34*, 179.
(57) Chen, J. G.; Kim, C. M.; Frühberger, B.; DeVries, B. E.; Touvelle, M. S. *Surf. Sci.* **1994**, *321*, 145.
(58) Chen, J. G.; Frühberger, B.; Eng, J., Jr.; Bent, B. E. *J. Mol. Catal. A* **1998**, *131*, 285.
(59) Dhandapani, B.; Ramanathan, S.; Yu, C. C.; Oyama, S. T.; Chen, J. G. *J. Catal.* **1998**, *176*, 61.
(60) Chen, J. G.; Eng, J., Jr.; Kelty, S. P. *Catal. Today* **1998**, *43*, 147.
(61) Kitchin, J. R. Ph.D. Thesis, Department of Chemical Engineering, University of Delaware, 2004.
(62) Price, D. L.; Wills, J. M.; Cooper, B. R. *Phys. Rev. Lett.* **1996**, *77*, 3375.
(63) Zhang, Y. F.; Li, J. Q.; Chen, W. K.; Zhou, L. X. *Acta Chim. Sin.* **2002**, *60*, 1798.
(64) Siegal, D. J.; Hector, L. G., Jr.; Adams, J. B. *Acta Mater.* **2002**, *50*, 619.
(65) Gauthier, Y.; Schmid, M.; Hebenstreit, W.; Varga, P. *Surf. Sci.* **2003**, *547*, 394.
(66) Tsong, R. M.; Schmid, M.; Nagl, C.; Varga, P.; Davis, R. F.; Tsong, I. S. T. *Surf. Sci.* **1996**, *366*, 85.
(67) Schöberl, T. *Surf. Sci.* **1995**, *327*, 285.
(68) Gall, N. R.; Rut'kov, E. V.; Tontegode, A. Ya. *Surf. Sci.* **2001**, *472*, 187.
(69) Potekhina, N. D.; Gall, N. R.; Rut'kov, E. V.; Tontegode, A. Y. *Phys. Solid State* **2003**, *45*, 782.
(70) Detroye, M.; Reniers, F.; Buess-Herman, C.; Vereecken, J. *Appl. Surf. Sci.* **1997**, *120*, 85.
(71) Tono, K.; Terasaki, A.; Ohta, T.; Kondow, T. *J. Chem. Phys.* **2002**, *117*, 7010.
(72) Tono, K.; Terasaki, A.; Ohta, T.; Kondow, T. *Chem. Phys. Lett.* **2002**, *351*, 135.
(73) Kobayashi, K.; Tsukada, M. *Phys. Rev. B* **1994**, *49*, 7660.
(74) Edamoto, K.; Nakane, T.; Noda, T.; Ozawa, K. *J. Electron Spectrosc. Relat. Phenom.* **1998**, *88*−*91*, 805.
(75) Hayami, W.; Souda, R.; Aizawa, T.; Otani, S.; Ishizawa, Y. *Surf. Sci.* **1996**, *346*, 158.
(76) Hayami, W.; Souda, R.; Aizawa, T.; Otani, S.; Ishizawa, Y. *Surf. Sci.* **1992**, *276*, 299.
(77) Tokumitsu, S.; Anazawa, T.; Ozawa, K.; Sekine, R.; Miyazaki, E.; Edamoto, K. *Phys. Rev. B* **1995**, *51*, 4516.
(78) Tokumitsu, S.; Anazawa, T.; Tanabe, A.; Sekine, R.; Miyazaki, E.; Edamoto, K.; Kato, H.; Otani, S. *Surf. Sci.* **1996**, *351*, 165.
(79) Edamoto, K.; Miyazaki, E.; Anazawa, T.; Mochida, A.; Kato, H. *Surf. Sci.* **1992**, *270*, 389.
(80) Aizawa, T.; Hayami, W.; Souda, R.; Otani, S.; Ishizawa, Y. *Surf. Sci.* **1997**, *381*, 157.
(81) Liu, N.; Kourtakis, K.; Figueroa, J.; Chen, J. G. *J. Catal.* **2003**, *215*, 254.
(82) Kato, S.; Ozawa, K.; Edamoto, K.; Otani, S. *Jpn. J. Appl. Phys.* **2000**, *39*, 5217.
(83) Noda, T.; Nakane, T.; Ozawa, K.; Edamoto, K.; Tanaka, S.; Otani, S. *Solid State Commun.* **1998**, *107*, 145.
(84) Oshima, C.; Otani, S.; Aono, M.; Zaima, S.; Shibata, Y. *Jpn. J. Appl. Phys.* **1983**, *22*, 930.
(85) Frantz, P.; Didziulis, S. V. *Surf. Sci.* **1998**, *412*/*413*, 384.
(86) Merrill, P. B.; Perry, S. S. *Surf. Sci.* **1998**, *418*, 342.
(87) Kuramochi, H.; Takami, K.; Saito, A.; Kuwahara, Y.; Mori, Y.; Otani, S.; Aono, M. *Appl. Phys. Lett.* **1999**, *75*, 3784.
(88) Ahn, J.; Kawanowa, H.; Souda, R. *Surf. Sci.* **1999**, *429*, 338.
(89) Brillo, J.; Kuhlenbeck, H.; Freund, H.-J. *Surf. Sci.* **1998**, *409*, 199.
(90) Håkansson, K. L.; Johansson, H. I. P.; Johansson, L. I. *Phys. Rev. B* **1994**, *49*, 2035.
(91) Aizawa, T.; Hayami, W.; Souda, R.; Otani, S.; Tanaka, T. *Surf. Sci.* **1996**, *357*, 645.
(92) St. Clair, T. P.; Oyama, S. T.; Cox, D. F. *Surf. Sci.* **2000**, *468*, 62.
(93) Leary, K. J.; Michaels, J. N.; Stacy, A. M. *J. Catal.* **1986**, *101*, 301.
(94) Hwu, H. H.; Chen, J. G. *Surf. Sci.* **2004**, *557*, 144.
(95) Liu, N.; Rykov, S. A.; Chen, J. G. *Surf. Sci.* **2001**, *487*, 107.
(96) Oshima, C.; Aono, M.; Tanaka, T.; Kawai, S.; Zaima, S.; Shibata, Y. *Surf. Sci.* **1981**, *102*, 312.
(97) Zaima, S.; Shibata, Y.; Adachi, H.; Oshima, C.; Otani, S.; Aono, M.; Ishizawa, Y. *Surf. Sci.* **1985**, *157*, 380.
(98) Souda, R.; Oshima, C.; Otani, S.; Ishizawa, Y.; Aono, M. *Surf. Sci.* **1988**, *199*, 154.
(99) Didziulis, S. V.; Frantz, P.; Fernandez-Torres, L. C.; Guenard, R.; El-bjeirami, O.; Perry, S. S. *J. Phys. Chem. B* **2001**, *105*, 5196.
(100) Chen, J. G.; DeVries, B. D.; Fruhberger, B.; Kim, C. M.; Liu, Z. M. *J. Vac. Sci. Technol., A* **1995**, *13*, 1600.
(101) Chen, J. G.; Weisel, M. D.; Liu, Z.-M.; White, J. M. *J. Am. Chem. Soc.* **1993**, *115*, 8875.
(102) Chen, J. G.; Colaianni, M. L.; Weinberg, W. H.; Yates, J. T., Jr. *Chem. Phys. Lett.* **1991**, *177*, 113.
(103) Sung, S.; Hoffmann, R. *J. Am. Chem. Soc.* **1985**, *107*, 578.
(104) Nakane, T.; Noda, T.; Ozawa, K.; Edamoto, K. *Surf. Sci.* **1999**, *435*, 180.
(105) Brillo, J.; Sur, R.; Kuhlenbeck, H.; Freund, H.-J. *Surf. Sci.* **1998**, *397*, 137.
(106) Brillo, J.; Sur, R.; Kuhlenbeck, H.; Freund, H.-J. *J. Electron Spectrosc. Relat. Phenom.* **1998**, *88*, 809.
(107) Hamnett, A. *Catal. Today* **1997**, *38*, 445.
(108) Parsons, R.; VanderNoot, T. *J. Electroanal. Chem.* **1988**, *257*, 9.
(109) Stonehart, P. In *Electrochemistry and Clean Energy*; Drake, J., Ed.; Royal Society of Chemistry: Cambridge, 1994.
(110) Hwu, H. H.; Chen, J. G. *J. Vac. Sci. Technol., A* **2003**, *21*, 1488.
(111) Hwu, H. H.; Polizzotti, B. D.; Chen, J. G. *J. Phys. Chem. B* **2001**, *105*, 10045.
(112) Hwu, H. H.; Chen, J. G. *J. Phys. Chem. B* **2003**, *107*, 2029.
(113) Ertl, G.; Neuman, M.; Streit, K. M. *Surf. Sci.* **1977**, *64*, 393.
(114) Crossley, A.; King, D. A. *Surf. Sci.* **1977**, *68*, 528.
(115) Kostov, K. L.; Rauscher, H.; Menzel, D. *Surf. Sci.* **1992**, *278*, 62.
(116) Bautier de Mongeot, F.; Scherer, M.; Gleich, B.; Kopatzki, E.; Behm, R. J. *Surf. Sci.* **1998**, *411*, 249.
(117) Ko, E. I.; Madix, R. J. *Surf. Sci.* **1981**, *109*, 221.
(118) Friend, C. M.; Serafin, J. G.; Baldwin, E. K.; Stevens, P. A.; Madix, R. J. *J. Chem. Phys.* **1987**, *87*, 1847.
(119) Edamoto, K.; Shiobara, E.; Anazawa, T.; Hatta, M.; Miyazaki, E.; Kato, H.; Otani, S. *J. Chem. Phys.* **1992**, *96*, 842.
(120) Zhang, M. H.; Hwu, H. H.; Buelow, M. T.; Chen, J. G.; Ballinger; T. H.; Andersen, P. J. *Catal. Lett.* **2001**, *77*, 29.
(121) Zhang, M. H.; Hwu, H. H.; Buelow, M. T.; Chen, J. G.; Ballinger, T. H.; Andersen, P. J.; Mullins, D. R. *Surf. Sci.* **2003**, *522*, 112.

(122) Baldwin, E. K.; Friend, C. M. *J. Phys. Chem.* **1987**, *91*, 3821.
(123) Blomberg, M. R. A.; Siegbahn, P. E. M.; Svensson, M. *J. Phys. Chem.* **1992**, *96*, 9794.
(124) Sheppard, N. *Annu. Rev. Phys. Chem.* **1988**, *39*, 589.
(125) Ko, E. I.; Madix, R. J. *Surf. Sci.* **1980**, *100*, L449.
(126) Frühberger, B.; Chen, J. G. *J. Am. Chem. Soc.* **1996**, *118*, 11599.
(127) Pearlstine, K. A.; Friend, C. M. *J. Vac. Sci. Technol., A* **1984**, *2*, 1021.
(128) Hwu, H. H.; Chen, J. G. *J. Phys. Chem. B* **2003**, *107*, 11467.
(129) Steininger, H.; Ibach, H.; Lehwald, S. *Surf. Sci.* **1982**, *117*, 685.
(130) Eng, J., Jr.; Chen, J. G.; Abdelrehim, I. M.; Madey, T. E. *J. Phys. Chem. B* **1998**, *102*, 9687.
(131) Gellman, A. J. *J. Am. Chem. Soc.* **1991**, *113*, 4435.
(132) Hoffmann, H.; Zaera, F.; Ormerod, R. M.; Lambert, R. M.; Yao, J. M.; Saldin, D. K.; Wang, L. P.; Bennett, D. W.; Tysoe, W. T. *Surf. Sci.* **1992**, *268*, 1.
(133) Abdelrehim, I. M.; Caldwell, T. E.; Land, D. P. *J. Phys. Chem.* **1996**, *100*, 10265.
(134) Avery, N. R. *J. Am. Chem. Soc.* **1985**, *107*, 6711.
(135) Lomas, J. R.; Baddeley, C. J.; Tikhov, M. S.; Lambert, R. M. *Langmuir* **1995**, *11*, 3048.
(136) Solymosi, F.; Bugyi, L.; Oszko, A. *Catal. Lett.* **1999**, *57*, 103.
(137) Solymosi, F.; Bugyi, L.; Oszko, A.; Horvath, I. *J. Catal.* **1999**, *185*, 160.
(138) Zaera, F. *J. Mol. Catal.* **1994**, *86*, 221.
(139) Bent, B. E. *Chem. Rev.* **1996**, *96*, 1361.
(140) Chen, J. G. *J. Catal.* **1995**, *154*, 80.
(141) Chen, J. G.; Frühberger, B.; Baumgartner, J.; DeVries, B. D. In *The Chemistry of Transition Metal Carbides and Nitrides*; Oyama, S. T., Ed.; Blackie Academic and Professional: Glasgow, 1996; p 439.
(142) Eng, J., Jr.; Frühberger, B.; Chen, J. G.; Bent, B. E. *Catal. Lett.* **1998**, *54*, 133.
(143) Avery, N. R.; Sheppard, N. *Proc. R. Soc. London, A* **1986**, *405*, 1.
(144) Chesters, M. A.; Horn, A. B.; Ilharco, L. M. *J. Electron Spectrosc. Relat. Phenom.* **1990**, *54*/*55*, 677.
(145) Eng, J., Jr.; Chen, J. G. *Surf. Sci.* **1998**, *414*, 374.
(146) Bugyi, L.; Oszko, A.; Solymosi, F. *Surf. Sci.* **2002**, *516*, 74.
(147) Bugyi, L.; Oszko, A.; Solymosi, F. *Surf. Sci.* **2002**, *519*, 139.
(148) Henn, F. C.; Diaz, A. L.; Bussell, M. E.; Hugenschimidt, M. B.; Domagala, M. E.; Campbell, C. T. *J. Phys. Chem.* **1992**, *96*, 5965.
(149) Bussell, M. E.; Henn, F. C.; Campbell, C. T. *J. Phys. Chem.* **1992**, *96*, 5978.
(150) Hwu, H. H.; Eng, J., Jr.; Chen, J. G. *J. Am. Chem. Soc.* **2002**, *124*, 702.
(151) Rodriguez, J. A.; Campbell, C. T. *J. Catal.* **1989**, *115*, 500.
(152) Chen, J. G.; Frühberger, B. *Surf. Sci.* **1996**, *367*, L102.
(153) Eng, J., Jr.; Bent, B. E.; Frühberger, B.; Chen, J. G. *Langmuir* **1998**, *14*, 1301.
(154) Zellner, M. B.; Chen, J. G. Unpublished results.
(155) Liu, N.; Rykov, S. A.; Hwu, H. H.; Buelow, M. T.; Chen, J. G. *J. Phys. Chem. B* **2001**, *105*, 3894.
(156) Polizzotti, B. D.; Hwu, H. H.; Chen, J. G. *Surf. Sci.* **2002**, *520*, 97.
(157) Sunderland, K. J.; Slavin, A. J. *Surf. Sci.* **1990**, *233*, 89.
(158) Iglesia, E.; Ribeiro, F. H.; Boudart, M.; Baumgartner, J. E. *Catal. Today* **1992**, *15*, 455.
(159) Iglesia, E.; Ribeiro, F. H.; Boudart, M.; Baumgartner, J. E. *Catal. Today* **1992**, *15*, 307.
(160) Pham-Huu, C.; Ledoux, M. J.; Guille, J. *J. Catal.* **1993**, *143*, 249.
(161) Blekkan, E. A.; Pham-Huu, C. C.; Ledoux, M. J.; Guille, J. *Ind. Eng. Chem. Res.* **1994**, *33*, 1657.
(162) Liu, N.; Chen, J. G. *Catal. Lett.* **2001**, *77*, 35.
(163) Hwu, H. H.; Frühberger, B.; Chen, J. G. *J. Catal.* **2004**, *221*, 170.
(164) Nakano, H.; Nakamura, J. *Surf. Sci.* **2001**, *482*, 341.
(165) Nakano, H.; Ogawa, J.; Nakamura, J. *Surf. Sci.* **2002**, *514*, 256.
(166) Kellogg, D. S.; Touvelle, M. S.; Stair, P. C. *J. Catal.* **1989**, *120*, 192.
(167) Teplyakov, A. V.; Bent, B. E.; Eng, J., Jr.; Chen, J. G. *Surf. Sci.* **1998**, *399*, L342.
(168) Pearlstine, K. A.; Friend, C. M. *J. Am. Chem. Soc.* **1985**, *107*, 5898.
(169) Abon, M.; Bertolini, J. C.; Billy, J.; Massardier, J.; Tardy, B. *Surf. Sci.* **1985**, *162*, 395.
(170) Surman, M.; Bare, S. R.; Hoffmann, P.; King, D. A. *Surf. Sci.* **1983**, *126*, 349.
(171) Grassian, V. H.; Muetterties, E. L. *J. Phys. Chem.* **1987**, *91*, 389.
(172) Eng, J., Jr.; Bent, B. E.; Frühberger, B.; Chen, J. G. *J. Phys. Chem. B* **1997**, *101*, 4044.
(173) Koel, B. E.; Crowell, J. E.; Bent, B. E.; Mate, C. M.; Somorjai, G. A. *J. Phys. Chem.* **1986**, *90*, 2949.
(174) Brillo, J.; Hammoudeh, A.; Kuhlenbeck, H.; Panagiotides, N.; Schwegmann, S.; Over, H.; Freund, H.-J. *J. Electron Spectrosc. Relat. Phenom.* **1998**, *96*, 53.
(175) Bugyi, L.; Oszko, A.; Solymosi, F. *Surf. Sci.* **2003**, *539,* 1.
(176) Kawata, K. *Surf. Coat. Technol.* **1992**, *54*/*55*, 604.
(177) Boving, H. J.; Hnitermann, H. E. *Tribol. Int.* **1990**, *23*, 129.
(178) Didziulis, S. V.; Frantz, P.; Perry, S. S.; El-bjeirami, O.; Imaduddin, S.; Merrill, P. B. *J. Phys. Chem. B* **1999**, *103*, 11129.
(179) Merrill, P. B.; Perry, S. S. *J. Phys. Chem. B* **1998**, *102*, 7606.
(180) Kitaoka, H.; Ozawa, K.; Edamoto, K.; Otani, S. *Solid State Commun.* **2001**, *118*, 23.
(181) Kitaoka, H.; Ozawa, K.; Edamoto, K.; Otani, S. *Surf. Sci.* **2002**, *518*, 225.
(182) Hwu, H. H.; Chen, J. G. *Surf. Sci.* **2003**, *536*, 75.
(183) Frantz, P.; Didziulis, S. V.; Fernandez-Torres, L. C.; Guenard, R. L.; Perry, S. S. *J. Phys. Chem. B* **2002**, *106*, 6456.
(184) Cotton, F. A.; Wilkinson, G. *Advanced Inorganic Chemistry*, 5th ed.; Wiley: New York, 1988.
(185) Zellner, M. B.; Hwu, H. H.; Chen, J. G. *Surf. Sci.*, submitted.
(186) Shinn, N. D. *Surf. Sci.* **1992**, *278*, 157.
(187) Erskine, J. L.; Bradshaw, A. M. *Chem. Phys. Lett.* **1980**, *72*, 260.
(188) Kojima, I.; Orita, M.; Miyazaki, E.; Otani, S. *Surf. Sci.* **1985**, *160*, 153.
(189) Hwu, H. H.; Chen, J. G.; Kourtakis, K.; Lavin, G. *J. Phys. Chem. B* **2001**, *105*, 10037.
(190) Sexton, B. A. *Surf. Sci.* **1981**, *102*, 271.
(191) Hrbek, J.; de Paola, R. A.; Hoffman, F. M. *J. Chem. Phys.* **1984**, *81*, 2818.
(192) Ko, E. I.; Benziger, J. B.; Madix, R. J. *J. Catal.* **1980**, *62*, 264.
(193) Guenard, R. L.; Fernández-Torres, L. C.; Kim, B.-I.; Perry, S. S.; Frantz, P.; Didziulis, S. V. *Surf. Sci.* **2002**, *515*, 103.
(194) Kim, B. I.; Lee, S.; Guenard, R.; Fernández-Torres, L. C.; Perry, S. S.; Frantz, P.; Didziulis, S. V. *Surf. Sci.* **2001**, *481*, 185.
(195) Fernández-Torres, L. C.; Kim, B.-I.; Perry, S. S. *Tribol. Lett.* **1997**, *3*, 239.
(196) Kim, H. I.; Frantz, P.; Didziulis, S. V.; Fernández-Torres, L. C.; Perry, S. S. *Surf. Sci.* **2003**, *543*, 103.
(197) Bugyi, L.; Oszko, A.; Solymosi, F. *Surf. Sci.* **2000**, *461*, 177.
(198) Liu, Z. M.; Solymosi, F.; White, J. M. *Surf. Sci.* **1991**, *245*, 289.
(199) Wohlrab, S.; Ehrlich, D.; Wambach, J.; Kuhlenbeck, H.; Freund, H.-J. *Vacuum* **1990**, *41*, 157.
(200) Hoffmann, F. M.; Weisel, M. D.; Paul, J. *Surf. Sci.* **1994**, *316*, 277.
(201) Benziger, J. B.; Ko, E. I.; Madix, R. J. *J. Catal.* **1979**, *58*, 149.
(202) Benziger, J. B.; Ko, E. I.; Madix, R. J. *J. Catal.* **1980**, *64*, 132.
(203) Barteau, M.; Madix, R. J. *J. Catal.* **1980**, *62*, 329.
(204) Topsoe, H.; Clausen, B. S.; Massoth, F. E. *Hydrotreating Catalysis, Science and Technology*; Springer: New York, 1996.
(205) Satterfield, C. N. *Heterogeneous Catalysis in Industrial Practice*; McGraw-Hill: New York, 1991.
(206) Thomas, J. M.; Thomas, W. J. *Principles and Practice of Heterogeneous Catalysis*; VCH: New York, 1997.
(207) Chianelli, R. R.; Lyons, J. E.; Mills, G. A. *Catal. Today* **1994**, *22*, 361.
(208) Sajkowski, D. J.; Oyama, S. T. *Appl. Catal. A* **1996**, *134*, 339.
(209) Kelly, D. G.; Salmeron, M.; Somorjai, G. A. *Surf. Sci.* **1986**, *175*, 465.
(210) St. Clair, T. P.; Oyama, S. T.; Cox, D. F. *Surf. Sci.* **2002**, *511*, 294.
(211) Rodriguez, J. A.; Dvorak, J.; Jirsak, T. *Surf. Sci.* **2000**, *457*, L413.
(212) Rodriguez, J. A.; Dvorak, J.; Jirsak, T. *J. Phys. Chem. B* **2000**, *104*, 11515.
(213) Stern, A. C.; Boubel, R. W.; Turner, D. B.; Fox, D. L. *Fundamentals of Air Pollution*, 2nd ed.; Academic Press: Orlando, FL, 1984.
(214) Roberts, J. T.; Friend, C. M. *Surf. Sci.* **1987**, *186*, 201.
(215) Wiegand, B. C.; Uvdal, P.; Friend, C. M. *Surf. Sci.* **1992**, *279*, 105.
(216) Roe, C. L.; Schulz, K. H. *Surf. Sci.* **2000**, *446*, 254.
(217) Roe, C. L.; Schulz, K. H. *J. Vac. Sci. Technol., A* **1998**, *16*, 1066.
(218) Roe, C. L.; Schulz, K. H. *Studies in Surface Science and Catalysis*; Elsevier: Amsterdam, 1999; Vol. 127, pp 121−128.
(219) Roberts, J. T.; Friend, C. M. *J. Phys. Chem.* **1988**, *92*, 5205.
(220) Rodriguez, J. A.; Liu, P.; Dvorak, J.; Jirsak, T.; Gomes, J.; Takahashi, Y.; Nakamura, K. *Surf. Sci.* **2003**, *543*, L675.
(221) Liu, P.; Rodriguez, J. A. *J. Chem. Phys.* **2003**, *119*, 10895.
(222) Rodriguez, J. A.; Jirsak, T.; González, L.; Evans, J.; Pérez, M.; Maiti, A. *J. Chem. Phys.* **2001**, *115*, 10914.
(223) Sayago, D. I.; Serrano, P.; Böhme, O.; Goldoni, A.; Paolucci, G.; Roman, E.; Martin-Gago, J. A. *Phys. Rev. B* **2001**, *64*, Art. No. 205402.
(224) Fernandez-Torres, L. C.; Perry, S. S.; Didziulis, S. V.; Frantz, P. P. *Surf. Sci.* **2002**, *511*, 121.
(225) Pearlstine, K. A.; Friend, C. M. *J. Phys. Chem.* **1986**, *90*, 4341.
(226) Serafin, J. G.; Friend, C. M. *J. Phys. Chem.* **1988**, *92*, 6694.
(227) Pearlstine, K. A.; Friend, C. M. *J. Phys. Chem.* **1986**, *90*, 4344.
(228) Friend, C. M.; Sarafin, J. G. *J. Chem. Phys.* **1988**, *88*, 4037.
(229) Reinke, P.; Oelhafen, P. *J. Appl. Phys.* **1997**, *81*, 2396.
(230) Schelz, S.; Kania, P.; Oelhafen, P.; Guntherodt, H.-J.; Richmond, T. *Surf. Sci.* **1995**, *359*, 227.
(231) Rodriguez, J. A.; Liu, P.; Dvorak, J.; Jirsak, T.; Gomes, J.; Takahashi, Y.; Nakamura, K. *Phys. Rev. B* **2004**, *69*, Art. No. 115414.
(232) Liu, P.; Rodriguez, J. A.; Muckerman, J. T. *J. Phys. Chem. B*, in press.

(233) Liu, P.; Rodriguez, J. A. *J. Chem. Phys.* **2004**, *11*, 5414.
(234) Hugosson, H. W.; Jansson, U.; Johansson, B.; Eriksson, O. *Chem. Phys. Lett.* **2001**, *333*, 444.
(235) Lightstone, J. M.; Mann, H. A.; Wu, M.; Johnson, P. M.; White, M. G. *J. Phys. Chem. B* **2003**, *107*, 10359.
(236) Duncan, M. A. *J. Cluster Sci.* **1997**, *8*, 239.
(237) Rohmer, M.-M.; Bénard, M.; Poblet, J.-M. *Chem. Rev.* **2000**, *100*, 495.
(238) Liu, P.; Rodriguez, J. A. *Catal. Lett.* **2003**, *91*, 247.
(239) Kitchin, J. R.; Nørskov, J. K.; Barteau, M. A.; Chen, J. G. *Phys. Rev. Lett.* **2004**, *93*, 156801.
(240) Hammer, B.; Nørskov, J. K. *Nature* **1995**, *376*, 238.
(241) Nørskov, J. K.; Bligaard, T.; Logadottir, A.; Bahn, S.; Hansen, L. B.; Bollinger, M.; Bengaard, H.; Hammer, B.; Sljivancanin, Z.; Mavrikakis, M.; Xu, Y.; Dahl, S.; Jacobsen, C. J. H. *J. Catal.* **2002**, *209*, 275.
(242) Kitchin, J. R.; Khan, N. A.; Barteau, M. A.; Chen, J. G.; Yakshinsky, B.; Madey, T. E. *Surf. Sci.* **2003**, *544*, 295.
(243) Kitchin, J. R.; Nørskov, J. K.; Barteau, M. A.; Chen, J. G. *J. Chem. Phys.* **2004**, *120*, 10240.
(244) Khan, N. A.; Hwu, H. H.; Chen, J. G. *J. Catal.* **2002**, *205*, 259.
(245) Khan, N. A.; Chen, J. G. *J. Vac. Sci. Technol., A* **2003**, *21*, 1302.
(246) Khan, N. A.; Zellner, M. B.; Chen, J. G. *Surf. Sci.* **2004**, *556*, 87.
(247) Mavrikakis, M.; Hammer, B.; Nørskov, J. K. *Phys. Rev. Lett.* **1998**, *81*, 2819.
(248) McCrea, K. R.; Logan, J. W.; Tarbuck, T. L.; Heiser, J. L.; Bussell, M. E. *J. Catal.* **1997**, *171*, 255.
(249) Darujati, A. R. S.; LaMont, D. C.; Thomson, W. J. *J. Appl. Catal. A* **2003**, *253*, 397.
(250) York, A. P. E.; Claridge, J. B.; Brungs, A. J.; Tsang, S. C.; Green, M. L. H. *Chem. Commun.* **1997**, *1*, 39.
(251) Claridge, J. B.; York, A. P. E.; Brungs, A. J.; Marquex-Alvarez, C.; Sloan, J. *J. Catal.* **1998**, *180*, 85.
(252) Skinner, P.; Howard, M. W.; Oxton, I. A.; Kettle, S. F. A.; Powell, D. B.; Sheppard, N. *J. Chem. Soc., Faraday Trans. 2* **1981**, *77*, 397.
(253) Siaj, M.; Reed, C.; Oyama, S. T.; Scott, S. L.; McBreen, P. H. *J. Am. Chem. Soc.* **2004**, *126*, 9514.

CR0204606